energies

IMPACT FACTOR 3.2

CITESCORE 5.5

Article

Communicationless Overcurrent Relays Coordination for Active Distribution Network Considering Fault Repairing Periods

Mahmoud A. Elsadd, Ahmed F. Zobaa, Heba A. Khattab, Ahmed M. Abd El Aziz and Tamer Fetouh

MDPI

https://doi.org/10.3390/en16237862

energies

MDPI

Article

Communicationless Overcurrent Relays Coordination for Active Distribution Network Considering Fault Repairing Periods

Mahmoud A. Elsadd [1], Ahmed F. Zobaa [2,*], Heba A. Khattab [3], Ahmed M. Abd El Aziz [3] and Tamer Fetouh [3]

[1] Electrical Engineering Department, Faculty of Engineering, Damanhour University, Damanhour 22511, Egypt; mahmoud.elsadd@dmu.edu.eg
[2] Electronic and Electrical Engineering Department, Brunel University London, Uxbridge UB8 3PH, UK
[3] Electrical Engineering Department, Faculty of Engineering, Menoufia University, Menoufia 32511, Egypt; ahmed_el_baiomy@yahoo.com (A.M.A.E.A.)
* Correspondence: azobaa@ieee.org

Abstract: This paper presents an integrated overcurrent relays coordination approach for an Egyptian electric power distribution system. The protection scheme suits all network topologies, including adding distribution generation units (DGs) and creating new paths during fault repair periods. The optimal types, sizes, and locations of DGs are obtained using HOMER software (Homer Pro 3.10.3) and a genetic algorithm (GA). The obtained values align with minimizing energy costs and environmental pollution. The proposed approach maintains dependability and security under all configurations using a single optimum setting for each relay. The calculations consider probable operating conditions, including DGs and fault repair periods. The enhanced coordination procedure partitions the ring into four parts and divides the process into four paths. The worst condition of two cascaded overcurrent relays from the DGs' presence viewpoint is generalized for future work. Moreover, a novel concept addresses the issue of insensitivity during fault repair periods. The performance is validated through the simulation of an Egyptian primary distribution network.

Keywords: adaptive coordination; directional relay; distributed generator; HOMER; photovoltaic (PV); wind turbine; fuel cell genetic algorithm; overcurrent protection

Citation: Elsadd, M.A.; Zobaa, A.F.; Khattab, H.A.; Abd El Aziz, A.M.; Fetouh, T. Communicationless Overcurrent Relays Coordination for Active Distribution Network Considering Fault Repairing Periods. *Energies* **2023**, *16*, 7862. https://doi.org/10.3390/en16237862

Academic Editor: Pavlos S. Georgilakis

Received: 22 September 2023
Revised: 18 November 2023
Accepted: 23 November 2023
Published: 30 November 2023

1. Introduction

The possession of advanced and stable electric power systems has become an urgent necessity for each country to keep pace with the industrial and technological development that is gripping the world in all walks of life [1]. Electrical energy demands are growing continuously, requiring an increase in generation capacity. This leads to a growing increase in generation costs, environmental pollution, and global warming. Therefore, system designers must search for alternative clean and economical sources. Also, the higher cost of transmission and distribution losses motivates system planners to use these alternatives as distributed generation units (DGs) in electrical distribution networks. The complication of protective device coordination in interconnected power subtransmission systems and deregulated distribution systems is intensively increasing due to continuous changes in the interconnected systems' topology [2]. These changes result from sustained load growth and the corresponding installation of distributed generation units (DGs). In recent times, various distributed generation units (DGs) have been integrated into interconnected power systems due to their advantages over installing remote generation stations [3,4]. To fully leverage the presence of DGs in the system, extensive studies have been conducted in the literature [5].

As per the survey conducted by Electric Power Research and Natural Gas Institutions, the electric power generation shared by distributed generation units (DGs) is estimated

to reach approximately 30% of the total power [6,7]. The types of DGs include small gas turbines, microturbines, fuel cells, wind, and solar energy. The literature has addressed the optimal allocation of DGs considering fuel cost savings and demand variation, as demonstrated in [8]. However, the integration of DGs has some adverse effects on the reliability and speed of the protection system [9]. The protection system may become unreliable due to incorrect operation or insensitivity (blinding) issues with protective devices. Slower protection system response (increased protection time) could result in exceeding the thermal capacity limit of electrical equipment, such as a transformer during close-in faults. These negative effects are influenced not only by changes in the level and direction of the fault current but also by the potential mismatch in fault current levels between coordinated relay pairs. On the other hand, another challenge for overcurrent relays coordination is ensuring the continuity of the distribution system by connecting the bus coupler (BC). If there is a fault in the feeder, the corresponding overcurrent relays would issue a tripping signal to isolate the fault. This leads to disconnecting healthy loads, especially when the fault is close to the upstream section. Connecting the BC ensures the supply of power to these loads from another direction. However, the direction and magnitude of current change in some sections, leading to relays miscoordination.

In [10], a coordination method utilizing directional overcurrent relays with nonstandard characteristics is presented to cancel the negative effect of the DGs' presence while enhancing the protection speed. In [11], a coordination technique based on a new coordination index determined by a two-phase nonlinear programming method is presented to reduce both the number of adaptive relays and the total operating time of the installed relays. In [12], an optimum coordination method considering the high penetration of DGs is presented, which reduces the total operating time by utilizing the adaptive modified firefly optimization algorithm.

Another trend to mitigate the effect of DGs on the reliability and speed of the protection system is by adding fault current limiters (FCLs), either in series with DGs or at different locations within the distribution sections [13,14]. In [15], the minimization of the FCLs values, with the permission to readjust the original setting of only one overcurrent relay, is accomplished. However, the techniques presented in [13–15] increase the cost due to the addition of FCLs.

In [16–19], the proper settings are selected, and the proper coordination is maintained by exchanging data between the agents installed at different points in electric distribution systems, such as DGs and relay locations, through the installed communication channels. In [16], an adaptive overcurrent relays coordination system activating the best settings for each operating condition is presented with the aid of the centralized control method (SCADA system) that monitors the system configuration and DGs status. Consequently, the centralized agent determines the corresponding optimum settings utilizing the differential evolution algorithm and then updates the relays' settings via the communication channels. In [17], the communication simulation of agents is enhanced, and the case of primary protection failure is covered by operating the nearest backup function. In [18], the adaptive overcurrent relays coordination covers the existence of both parallel feeders and DGs presence by exchanging the data on both the operating condition of the two parallel feeders and the current direction of these feeders. In [19], the negative effect of DGs' presence on overcurrent relay–recloser–fuse protection of distribution systems is cancelled by transferring the measured currents at fuse locations to select the adequate setting of the fast curve of the recloser.

Recently, there has been a growing interest in implementing intelligent methods in protection systems by utilizing communication infrastructure and intelligent electronic devices (IEDs). Notably, various intelligent techniques have been highlighted in [20–24], employing multi-agent systems (MASs). These MASs enable the exchange of distribution network data among agents, thereby enhancing the protection system's performance. For instance, in [20], an intelligent protection scheme is presented, which utilizes a centralized and multilayered MAS to interact with relays, DGs, and loads, ensuring effective

protection coordination. Another approach, detailed in [21], introduces a MAS-based self-healing protection scheme that adapts to varying network conditions. Furthermore, Ref. [22] introduces a self-healing protection system utilizing a MAS comprising feeder, zone, breaker, and DG agents. Additionally, Ref. [23] proposes a protection system that combines MAS and machine learning algorithms to coordinate and update the protection scheme, allowing adaptation to new network conditions. In [24], the proper delaying time is activated through communication between the neighboring relays. It is essential to consider that the performance of MAS-based protection systems is significantly influenced by the implementation of communication links between agents, as well as the number and type of agents involved. Additionally, the reliability of the protection system depends on the communication system's reliability, which can be affected by both cyberattacks and the risk of communication failures. Consequently, the complexity of coordinating the relays without the need for communications, while considering both the busbar coupler operation and the self-healing process (during fault repairing periods), represents a challenge for protection engineers, particularly in the presence of multiple DGs.

The main contribution of this paper is presenting a novel coordination approach to maintain both dependability and security attributes for active distribution systems. This approach considers fault repair periods and the presence of multiple DGs, while utilizing a single optimum setting for each relay. The coordination procedure is based on partitioning the ring into four parts and dividing the process into four paths (four subroutine algorithms). The worst condition of each two cascaded overcurrent relays from the viewpoint of DGs is generalized for future work. Additionally, a new idea overcomes the insensitivity problem during fault repair. The performance of the proposed approach is examined through the simulation of an actual Egyptian primary distribution network.

The content of the following sections is outlined as follows: the illustration of the test system is in Section 2. The optimal allocation of distributed generation units is presented in Section 3, which includes both the HOMER-based model for selecting suitable DGs and DG sizing in Section 3.1, and the GA-based model for DG siting in Section 3.2. Conventional overcurrent relays coordination is discussed in Section 4, covering the procedure of conventional coordination in Section 4.1 and the effect of DGs' presence on conventional coordination in Section 4.2. Section 5 introduces the modified overcurrent relays coordination for distribution systems with distributed generation units, including coordination of forward relays, coordination of backward relays, and the evaluation of the modified coordination under opening bus coupler in Sections 5.1–5.3, respectively. To consider fault repairing periods, including the case of closing bus coupler, a new communicationless overcurrent relays coordination approach for deregulated distribution systems is introduced in Section 6. Section 6.1 illustrates the concept of the proposed communicationless Overcurrent Relays Coordination, while Section 6.2 illustrates the procedure for the computation of the new coordination approach. Section 7 contains the evaluation of the new protection coordination approach. Finally, the conclusion is presented in Section 8.

2. Test System

In this paper, an 11 kV primary distribution network located in Sadat City is used as an actual test system, as shown in Figure 1. The network has 30 busbars, divided into two feeders with a total load of 10.054 MW and 7.8 MVAR. The system data are given in Appendix A. Load flow calculations are carried out, and their results indicate the presence of four overloaded sections (1–2, 1–15, 15–16, and 16–17) with power losses of 133.9 kW. To relieve the overloaded lines and minimize the power losses in the considered system, an optimal allocation study for adding distributed generation units is accomplished in the next section.

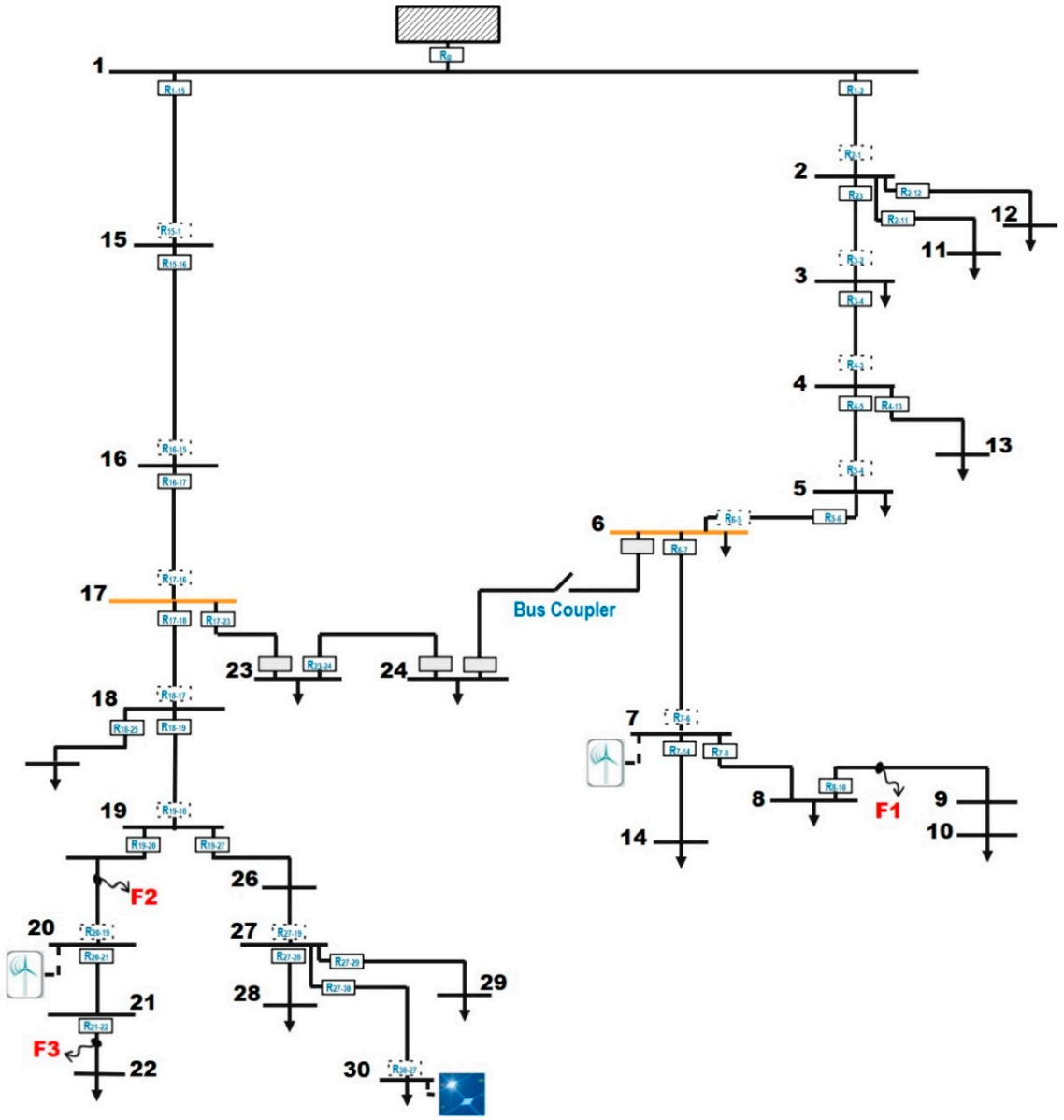

Figure 1. Actual Egyptian distribution network showing both forward and backward relays.

3. Optimal Allocation of Distributed Generation Units

The incorporation of distributed generation units (DGs) into distribution networks involves two main issues. The first issue is determining the type and penetration level of each DG, considering economic and emission performance within the system. This aspect is addressed using HOMER software, which focuses on the generation units and load of the network, regardless of the network configuration. HOMER software optimally selects suitable DGs and determines their penetration level. The second issue involves determining the optimal location for each DG unit within the distribution network. This problem is treated using a genetic algorithm, which serves as an optimization tool to find the optimal locations of the DG units while considering various network constraints. These issues are summarized in the flowchart illustrated in Figure 2.

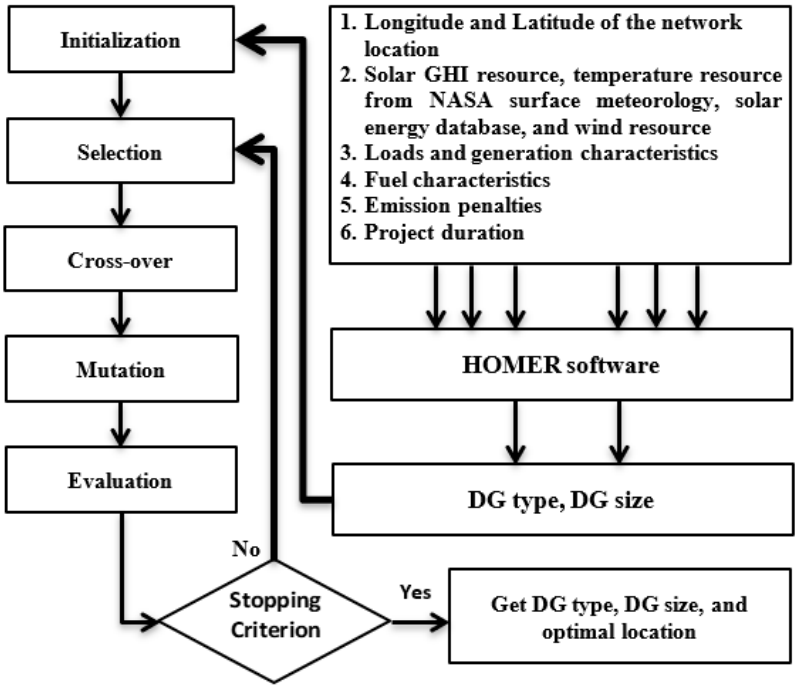

Figure 2. Determination of optimal allocation for distributed generation units: a step-by-step process.

3.1. HOMER-Based Model for Selecting Suitable DGs and DG Sizing

The objective is to minimize the total energy cost (COE) supplied to the loads by DGs in conjunction with the grid, utilizing HOMER software. The overall cost is expressed as follows [25]:

$$C_{total} = C_{grid} + C_{PV} + C_{WT} + C_D + C_{FC} + C_{Batt.} + C_{inv} - C_{sold\ E} \quad (1)$$

where:

C_{grid} is the cost of energy used from the grid ($).
C_{PV} is the photovoltaic arrangement cost ($).
C_{WT} is the wind turbine cost ($).
C_D is the diesel generator cost ($).
C_{FC} is the fuel cell cost ($).
$C_{Batt.}$ is the battery bank cost ($).
C_{inv} is the cost of the inverter ($).
$C_{sold\ E}$ is the cost of energy delivered to the grid ($).

The cost function of the *i*th *DG* is formulated as [26]:

$$C_i = N_i \cdot \left[C_{cap,i} + O\&M_i + K_i \cdot C_{rep,i} - S_i\right] \quad (2)$$

where:

N_i is the number of inserted *DG*.
$C_{cap,i}$ is the capital cost of *DG* ($).
$O\&M_i$ is the operation and maintenance cost of *DG* ($).
K_i is the number of replacements for *DG*.
$C_{rep,i}$ is the replacement cost of *DG* ($).
S_i is the salvage amount of *DG* ($).

The constraints are listed in the following equations.

$$P_{DG(i)}{}^{min} \le P_{DG(i)} \le P_{DG(i)}{}^{max} \quad (3)$$

$$\sum_{i=1}^{N} P_{DG(i)} + P_{grid} = P_{LD} \quad (4)$$

where:

$P_{DG(i)}$ is the output power of *DG* (kW).
P_{grid} is the grid power (kW).
P_{LD} is the load demand (kW).

HOMER considers the network in two parts: generators and loads, while ignoring losses. Various types of DGs could be installed, such as photovoltaic (PV), wind turbine (WT), fuel cell (FC), batteries (B), and diesel generators (D). Each DG has its own characteristics that must be defined. Additionally, the load curve must be carefully defined for accurate DG sizing. Four steps are required to model a system in HOMER:

1. Obtaining the longitude and latitude of the network location.
2. Downloading the Solar Global Horizontal Irradiance (GHI) resource, temperature resource from NASA surface meteorology, solar energy database, and wind resource [27].
3. Adding the characteristics of both loads and generation.
4. Defining the fuel characteristics, the emission penalties, and finally the project duration.

By implementing these steps in the Egyptian distribution network, five DG units (WT, PV, Diesel, FC, and battery bank) can be simulated utilizing HOMER. The grid and DG standards are as follows:

- The grid power price and grid sellback price are 0.087 \$/kWh.
- The solar system is composed of stationary flat-plate PV with a lifetime of 25 years and an 80% derating factor. The maximum available space for PV is 1000 kW, obtained by utilizing the ready area to install a PV substation at the studied network location, where each kW requires a minimum area of 10 m^2. The Solar Global Horizontal Irradiance (GHI) resource is depicted in Figure 3.
- The Gamesa G126-2.5MW wind turbine with a lifetime of 20 years is utilized. Its hub height is 102 m, and the power curve of the wind turbine is illustrated in Figure 4. The average wind speed per year is 4.85 m/s [28].
- A diesel generator with a maximum available space of 1000 kW is utilized; however, the price of diesel fuel is 299×10^{-3} \$/L.
- A general fuel cell with a maximum available area of 100 kW is utilized, where hydrogen is used as fuel. The electrolyzer and hydrogen tank are utilized to supply the fuel cell with the hydrogen needed to operate.
- A battery bank, modified kinetic battery model, with a voltage of 2 V and a capacity of 1 kWh using a maximum available area of 30 batteries is utilized.
- Carbon dioxide needs to be removed from the atmosphere [29].

On the other hand, the load standards of the studied Egyptian distribution network consist of 10.054 MW, with the load profile illustrated in Figure 5. Figure 6 depicts the system in the HOMER software. The costs of the system components, including initial, replacement, operation, and maintenance, are listed in Table 1. The study is conducted for 20 years, which is the average lifetime of the considered components. The optimum types and sizes of DGs are obtained using HOMER, as listed in Table 2.

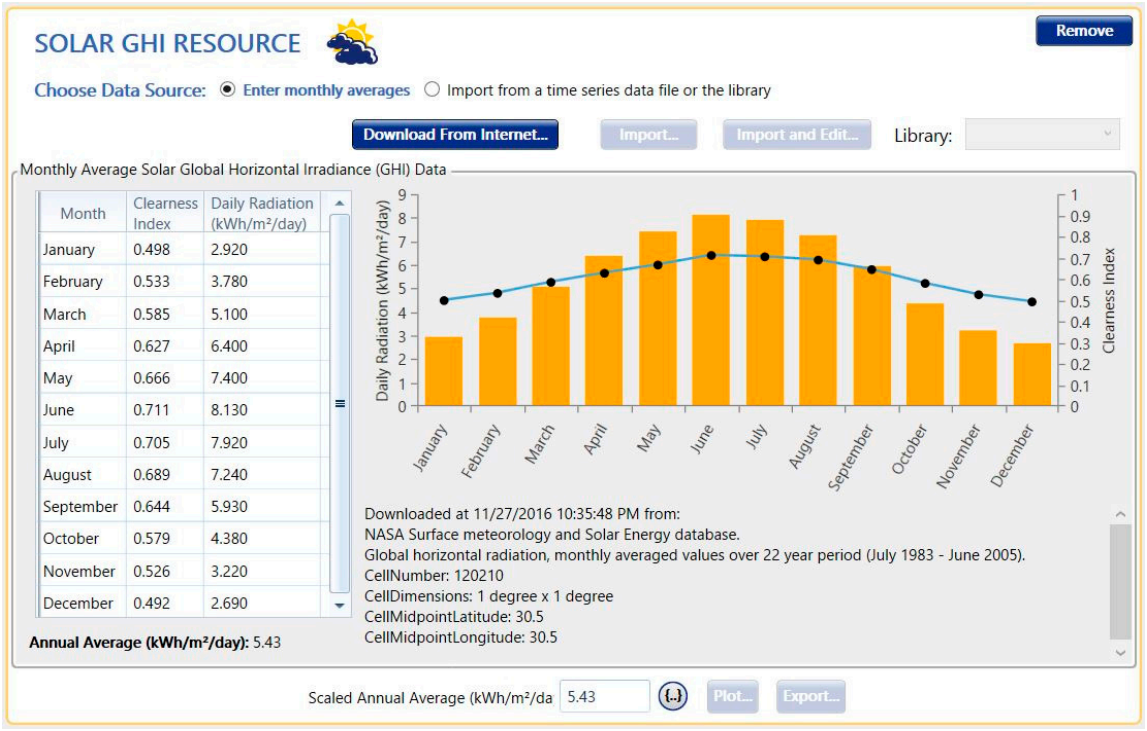

Figure 3. Average solar global horizontal irradiance (GHI) data per month.

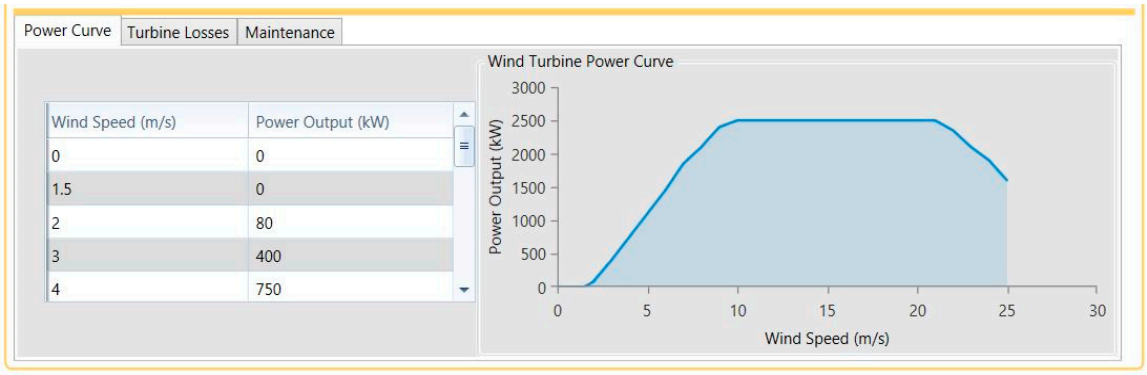

Figure 4. Gamesa G126 power curve.

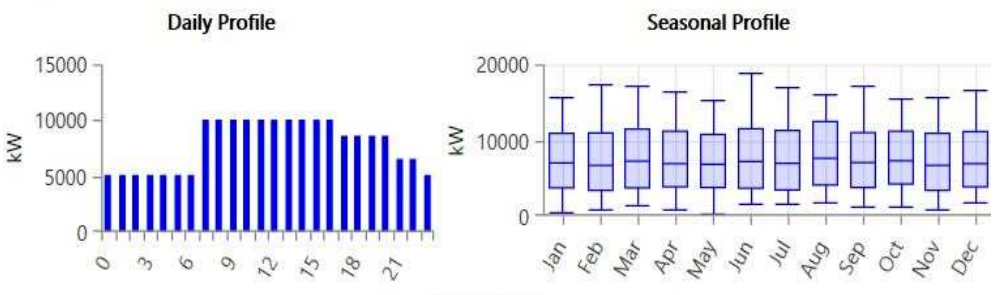

Figure 5. Load curve and its variation throughout the year.

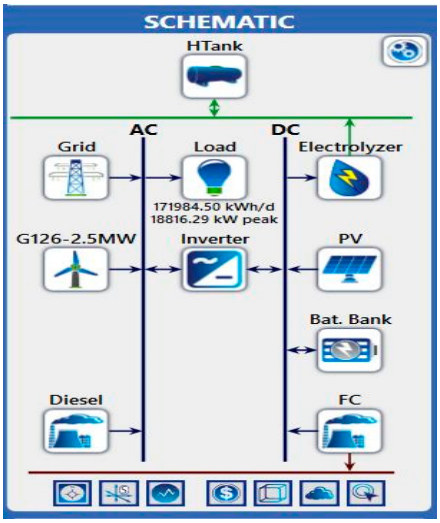

Figure 6. The system modeled on HOMER.

Table 1. The costs of the system components.

Component (Capacity/Quantity)	Capital Cost ($)	Replacement Cost ($)	Operation & Maintenance Cost ($)
PV (1 kW)	0.9×10^3	0.9×10^3	0
WT (2.5 MW)	5.5×10^6	5.5×10^6	9×10^4/year
Diesel (1 kW)	0.5×10^3	0.5×10^3	0.03/h
FC (1 kW)	3×10^3	2.5×10^3	0.01/h
Battery (2 V)	0.3×10^3	0.3×10^3	10/year
Electrolyzer (0.15 kW)	0.6×10^3	0.6×10^3	2/year
Hydrogen Tank (1 kg)	0.02×10^3	0.02×10^3	0.05/year

Table 2. HOMER optimization results.

Items		Optimum Results
Architecture	PV (kW) WT (G126—2.5 MW) Inverter (kW)	1000 2 680
Cost	COE ($/kWh) NPC ($) Operating cost ($) Initial capital ($)	0.0861 63 M 4.39 M 12.1 M
System	Renewable fraction (%)	33.6
PV	Capital cost ($) Production (kWh)	900,000 1,540,204
WT (G126—2.5 MW)	Capital cost ($) Production (kWh) O&M cost ($)	11,000,000 19,717,122 180,000
Grid	Energy purchased (kWh) Energy sold (kWh)	41,921,056 361,485

3.2. GA-Based Model for DG Siting

The output of the HOMER-based model is the optimal types and sizes of the DG units that improve the economic and emission performance of the Egyptian distribution network. The selected types of DG units should be optimally sited across the distribution

network, considering the configuration and operation constraints. GA is applied as a well-established optimization technique to handle the siting problem of the DG units in the distribution network. The main objective of the optimization problem is to minimize the total power loss while maintaining voltage regulation within a safe range in the primary distribution network. This optimization problem can be formulated as follows:

The objective function,

$$Minimize\ P_{loss} = \sum_{k=1}^{nl} Ploss_k \tag{5}$$

The objective function is subjected to the following constraints:

$$P_{grid} + \sum_{i=1}^{N} P_{DG} = P_{LD} + P_{loss} \tag{6}$$

$$V_i^{min} \leq V_i \leq V_i^{max} \tag{7}$$

where the power losses in the network are computed based on the Forward–Backward Sweep algorithm using the following equation:

$$Ploss_k = R_k \left[\left(\sum_{j=2}^{nb} BIBC(k, j-1) \cdot \frac{P_j\ cos\theta_j + Q_j\ sin\theta_j}{|V_j|} \right)^2 + \left(\sum_{j=2}^{nb} BIBC(k, j-1) \cdot \frac{P_j\ sin\theta_j - Q_j\ cos\theta_j}{|V_j|} \right)^2 \right] \tag{8}$$

where:

$Ploss_k$ is the active power loss of branch k.
$BIBC$ is the Bus-Injection to Branch-Current matrix.
nl is the number of distribution system branches.
nb is the number of the distribution system buses.
V_j is the voltage magnitude at bus j.
θ_j is the voltage angle at bus j.
P_j is the net consumed active power at bus j.
Q_j is the net consumed reactive power at bus j.

GA is initialized with a population of random guesses that will be spread throughout the search space by applying three operators: selection, crossover, and mutation to generate new populations until reaching the optimal solution. GA is commonly utilized to solve various optimization problems in power systems. The total power loss in the network is treated as the objective function that needs to be minimized during the optimization process. Both the objective function and network constraints are calculated using the Forward–Backward Sweep algorithm.

The control variables of the optimal siting problem are the location and the output power generation of the DG units. The location control variable represents the busbar number, ranging from 2 up to the maximum number of buses in the distribution network. However, the DG output power control variable ranges from the minimum to the maximum power generation of each DG unit.

The results obtained from the GA-based DG siting algorithm show that siting the first WT at busbar 7, siting the second WT at busbar 20, and siting the PV station at busbar 30 are the optimal locations for the DG units. The total power loss decreased from 133.9 kW to 61.1 kW. The overloaded sections were relieved due to the optimal siting of the selected DGs.

4. Conventional Overcurrent Relays Coordination

The default configuration of the selected distribution system is that the bus coupler is disconnected, and no DGs are connected to the system. Therefore, an overcurrent relay upstream of each section is sufficient. Each relay is defined by two numbers. The first number represents the sending busbar, and the second one represents the receiving busbar. For example, for feeder (1-2), $R_{1\text{-}2}$ is the forward relay, as illustrated in Figure 1. To assess the effect of DGs penetration on conventional coordination, the procedure for conventional coordination should be performed as described in the following subsection.

4.1. The Procedure of the Conventional Coordination

The procedure for the conventional coordination between two cascaded inverse relays is detailed and illustrated in [18] by the same author. The Genetic Algorithm (GA) is utilized to verify the optimal coordination margins by minimizing the objective function, which is the sum of the operating times of the relays at the corresponding worst conditions. The objective function is verified under security constraints that ensure proper coordination between each pair of cascaded relays. The coordination constraints are incorporated into the objective function through an augmented fitness function, as shown in [18] by the same author. Initially, the coordination of the right-hand-side (RHS) relays from $R_{8\text{-}10}$ to $R_{1\text{-}2}$ in the considered system, as shown in Figure 1, is as follows: The downstream relays ($R_{2\text{-}11}$, $R_{2\text{-}12}$, $R_{4\text{-}13}$, $R_{7\text{-}14}$, $R_{8\text{-}10}$) are set to their lowest time dial setting (0.02 in numerical relays). The coordination constraint between relays $R_{7\text{-}8}$ and $R_{8\text{-}10}$ (downstream relays) is formulated as an inequality constraint (Z_{CTI}) using the maximum jointed fault current, as follows:

$$Z_{CTI1} = max\{0\,,\ (minCTI - (t_{R7-8} - t_{R8-10}))\} \tag{9}$$

Then, each pair of relays (11 pairs of relays) will be coordinated according to the maximum jointed fault current in the overlapped region, primarily protected by the inverse characteristic, for each pair of cascaded relays as shown in Table 3.

Table 3. Maximum jointed fault current for each two cascaded pairs of relays of the RHS feeder.

No. of Pairs	Pair of Relays		I_{Fmax} (For Phase Faults) (A)	I_{Fmax} (For Earth Faults) (A)
	Backup	Primary		
1	$R_{7\text{-}8}$	$R_{8\text{-}10}$	4596.4	4133.6
2	$R_{6\text{-}7}$	$R_{7\text{-}8}$	4696.3	4266.2
3	$R_{6\text{-}7}$	$R_{7\text{-}14}$	4711.4	4286.2
4	$R_{5\text{-}6}$	$R_{6\text{-}7}$	4769.1	4365.6
5	$R_{4\text{-}5}$	$R_{5\text{-}6}$	4874.4	4512.9
6	$R_{3\text{-}4}$	$R_{4\text{-}5}$	4941.6	4608.8
7	$R_{3\text{-}4}$	$R_{4\text{-}13}$	4943.7	4612.3
8	$R_{2\text{-}3}$	$R_{3\text{-}4}$	4969.5	4649.3
9	$R_{1\text{-}2}$	$R_{2\text{-}3}$	5028.3	4736
10	$R_{1\text{-}2}$	$R_{2\text{-}11}$	5037.5	4750
11	$R_{1\text{-}2}$	$R_{2\text{-}12}$	5038.4	4751.3

Finally, the fitness function for evaluating an individual in the population of the GA, containing the coordination margin among all relays in the RHS feeder, is:

$$fitness = \sum_{i=1}^{N} t_i + \sum_{j=1}^{11} K_j \cdot Z_{CTIj} \tag{10}$$

where '*i*' refers to the relay number, and '*j*' refers to the number of pairs, which ranges from 1 to 11 as indicated in Table 3. K_1 is selected to be equal to 8, K_2 and K_4 are set to 6, K_3, K_7, K_8, K_9, K_{10}, and K_{11} are all set to 3, K_5 is set to 5, and K_6 is set to 3.4. The physical meaning of using K_j is that these arbitrary factors guarantee the achievement of the coordination constraint by making their expression significant in the fitness function formula. Also, one can conclude that the violation constraint term equals zero upon achieving the coordination pair constraint. The maximum number of generations is set to 500, the generation gap is

0.8, the mutation rate depends on the number of variables, and a single crossover rate is assigned in the GA.

The best fitness function value is 5.862 s, and the corresponding values of time dial settings (*TDSs*) and pickup currents (I_{Ps}) that verify this optimal value are presented in Table 4. Similarly, the I_{Ps} and *TDSs* of the earth units are also listed in Table 4, calculated using the line-to-ground fault current.

Table 4. The obtained settings of the relays of the RHS feeder.

Relays	For Phase Faults		For Earth Faults	
	I_P (A)	TDS	I_P (A)	TDS
$R_{8\text{-}10}$	73	0.02	15	0.02
$R_{7\text{-}8}$	110	0.1287	22	0.1763
$R_{7\text{-}14}$	74	0.02	15	0.02
$R_{6\text{-}7}$	183	0.2065	37	0.3003
$R_{5\text{-}6}$	204	0.2923	41	0.4334
$R_{4\text{-}5}$	240	0.3657	48	0.5541
$R_{4\text{-}13}$	37	0.02	8	0.02
$R_{3\text{-}4}$	276	0.4331	56	0.6663
$R_{2\text{-}3}$	313	0.495	63	0.7761
$R_{2\text{-}11}$	37	0.02	8	0.02
$R_{2\text{-}12}$	37	0.02	8	0.02
$R_{1\text{-}2}$	385	0.5325	77	0.8612

Similarly, the coordination of the left-hand-side (LHS) relays from both $R_{27\text{-}30}$ and $R_{21\text{-}22}$ to $R_{1\text{-}15}$ in the depicted system (Figure 1) is completed. Each pair of relays is coordinated according to the maximum jointed fault current, as shown in Table 5. Additionally, the fitness function for evaluating each individual in the GA population, which includes the coordination margins among all relays in the LHS feeder using the currents listed in Table 5, is as follows:

$$fitness = \sum_{i=1}^{N} t_i + \sum_{j=1}^{14} K_j \cdot Z_{CTIj} \quad (11)$$

where '*j*' refers to the number of pairs, ranging from 1 to 14 as indicated in Table 5. The arbitrary factor K_1 is selected to be 7, K_2 and K_4 are set to 6, K_3, K_7, K_9, and K_{10} are all set to 3, K_5 is set to 5, K_6 and K_{14} are set to 4, K_8 is set to 3.025, K_{11} is set to 8, K_{12} is set to 2.6, and K_{13} is set to 2. The maximum number of generations is set to 500, the generation gap is 0.8, the mutation rate depends on the number of variables, and a single crossover rate is assigned in the GA.

Table 5. Maximum jointed fault current for each two cascaded pairs of relays of the LHS feeder.

No. of Pairs	Pair of Relays		I_{Fmax} (For Phase Faults) (A)	I_{Fmax} (For Earth Faults) (A)
	Backup	Primary		
1	$R_{19\text{-}27}$	$R_{27\text{-}28}$	4538.3	4036.5
2	$R_{19\text{-}27}$	$R_{27\text{-}29}$	4538.3	4036.5
3	$R_{19\text{-}27}$	$R_{27\text{-}30}$	4538.3	4036.5
4	$R_{20\text{-}21}$	$R_{21\text{-}22}$	4596.2	4103.4
5	$R_{19\text{-}20}$	$R_{20\text{-}21}$	4516.7	4129.9
6	$R_{18\text{-}19}$	$R_{19\text{-}20}$	4662.5	4197.4
7	$R_{18\text{-}19}$	$R_{19\text{-}27}$	4646.1	4177.3
8	$R_{17\text{-}18}$	$R_{18\text{-}19}$	4714	4439
9	$R_{17\text{-}18}$	$R_{18\text{-}25}$	4874.3	4492.6
10	$R_{17\text{-}23}$	$R_{23\text{-}24}$	4710.7	4284.5
11	$R_{16\text{-}17}$	$R_{17\text{-}23}$	4984.9	4655.7
12	$R_{16\text{-}17}$	$R_{17\text{-}18}$	5006.6	4683.4
13	$R_{15\text{-}16}$	$R_{16\text{-}17}$	5149.4	4896.2
14	$R_{1\text{-}15}$	$R_{15\text{-}16}$	5286.9	5106.7

The best fitness function value is 6.2137 s, and the corresponding values of the *TDSs* and I_{Ps} that verify this optimal value are provided in Table 6. Similarly, the I_{Ps} and *TDSs* of the earth units are also listed in Table 6, calculated using the line-to-ground fault current. However, the presence of DGs has negative effects on this conventional coordination, as illustrated in the following subsection.

Table 6. The obtained settings of the relays of the LHS feeder.

Relays	For Phase Faults		For Earth Faults	
	I_P (A)	TDS	I_P (A)	TDS
R_{27-28}	37	0.02	8	0.02
R_{27-29}	37	0.02	8	0.02
R_{27-3}	37	0.02	8	0.02
R_{19-27}	110	0.1257	22	0.1736
R_{21-22}	22	0.02	5	0.02
R_{20-21}	95	0.1296	19	0.178
R_{19-20}	168	0.2071	34	0.3019
R_{18-19}	278	0.2579	56	0.3982
R_{18-25}	37	0.02	8	0.02
R_{17-18}	314	0.3261	63	0.5139
R_{23-24}	37	0.02	8	0.02
R_{17-23}	73	0.1412	15	0.189
R_{16-17}	385	0.3767	77	0.6113
R_{15-16}	421	0.4368	85	0.7169
R_{1-15}	458	0.4936	92	0.822

4.2. The Effect of DGs Presence on the Conventional Coordination

To evaluate conventional protection in the presence of DGs, various fault scenarios at different locations are selected. These locations include section 8-9 representing F1, section 19-20 representing F2, and section 21-22 representing F3, as illustrated in Figure 1. Different miscoordination cases occurred under both phase and earth faults, as shown in Tables 7 and 8, respectively. These cases are analyzed as follows.

Assuming a solid three-phase fault (F1) downstream of relay R_{8-10} in section 8-10, two cases are simulated: one with and one without a Wind Turbine (WT) inserted at busbar 7. The study concludes that interconnecting a WT in the network leads to relay miscoordination. This is because the operating time (t_{op}) of relay R_{7-8} is longer than that of relay R_{8-10}. However, the time difference between these relays is lower than the coordination time interval (*CTI*), causing relay R_{7-8} to maloperate, as indicated by the shaded cells in Table 7. Similarly, for fault scenario F2, various cases are examined: without any distributed generators (DGs), with only a WT inserted at busbar 20, with only Photovoltaic (PV) inserted at busbar 30, and with all DGs inserted. The results show that interconnecting a WT without PV in the network leads to relay miscoordination. This occurs because relay R_{18-19} maloperates since the time difference between the operation times of relay R_{18-19} and relay R_{19-20} is less than *CTI*, resulting in a trip signal, as shown by the shaded cells in Table 7.

Additionally, under fault scenario F3, various cases are studied to cover all possible network topologies. The results indicate that interconnecting only PV or both DGs in the network leads to relay miscoordination. This is due to the time difference between the operation times of the backup relay (R_{19-20}) and the primary relay (R_{20-21}) being less than *CTI*, as noted in Table 7 by the shaded cells. The issue of miscoordination becomes more significant with an increase in the level of DGs.

Table 7. The effect of DGs presence on both the conventional and modified settings of the phase overcurrent relays' function.

Fault	Network Topology		Relay	I_F (A)	Conventional Coordination		Modified Coordination	
	WT	PV			Operating Time (s)	Miscoordination	Operating Time (s)	Miscoordination
F_1	—	—	$R_{8\text{-}10}$	4596.4	0.032415	—	0.032415	—
			$R_{7\text{-}8}$	4596.4	0.232466		0.236621	
	√	—	$R_{8\text{-}10}$	4944.7	0.03183	√	0.03183	—
			$R_{7\text{-}8}$	4944.7	0.227836		0.231908	
F_2	—	—	$R_{19\text{-}20}$	4662.5	0.421881	—	0.436548	—
			$R_{18\text{-}19}$	4662.5	0.622365		0.637327	
	√	—	$R_{19\text{-}20}$	4703	0.420749	√	0.435315828	—
			$R_{18\text{-}19}$	4703	0.620408		0.635394947	
	—	√	$R_{19\text{-}20}$	5011.4	0.412614	—	0.426959	—
			$R_{18\text{-}19}$	4664.6	0.622263		0.637222	
	√	√	$R_{19\text{-}20}$	5055	0.411528	—	0.425835	—
			$R_{18\text{-}19}$	4705.6	0.620283		0.635195	
F_3	—	—	$R_{20\text{-}21}$	4516.7	0.22597	—	0.233816	—
			$R_{19\text{-}20}$	4516.7	0.42609		0.440841	
	√	—	$R_{20\text{-}21}$	4979.6	0.220183	—	0.227829	—
			$R_{19\text{-}20}$	4655.3	0.422084		0.436697	
	—	√	$R_{20\text{-}21}$	4959.1	0.220422	√	0.228076	—
			$R_{19\text{-}20}$	4959.1	0.413936		0.428267	
	√	√	$R_{20\text{-}21}$	5326.7	0.216351	√	0.223863	—
			$R_{19\text{-}20}$	5002.2	0.412845		0.427138	

Table 8. The effect of DGs presence on both the conventional and modified settings of the earth overcurrent relays' function.

Fault	Network Topology		Relay	I_F (A)	Conventional Coordination		Modified Coordination	
	WT	PV			Operating Time (s)	Miscoordination	Operating Time (s)	Miscoordination
F_1	—	—	$R_{8\text{-}10}$	4133.6	0.023542	—	0.023542	—
			$R_{7\text{-}8}$	4133.6	0.223576		0.225985	
	√	—	$R_{8\text{-}10}$	4387.7	0.023281	√	0.023281	—
			$R_{7\text{-}8}$	4387.7	0.220923		0.223304	
F_2	—	—	$R_{19\text{-}20}$	4197.4	0.418027	—	0.425366	—
			$R_{18\text{-}19}$	4197.4	0.618227		0.626766	
	√	—	$R_{19\text{-}20}$	4298.7	0.415867	√	0.423167	—
			$R_{18\text{-}19}$	4298.7	0.614681		0.623171	
	—	√	$R_{19\text{-}20}$	4453.1	0.412708	—	0.419954	—
			$R_{18\text{-}19}$	4287.3	0.615074		0.62357	
	√	√	$R_{19\text{-}20}$	4550.8	0.410788	—	0.418	—
			$R_{18\text{-}19}$	4381.1	0.611886		0.620338	
F_3	—	—	$R_{20\text{-}21}$	4129.9	0.219294	—	0.223976	—
			$R_{19\text{-}20}$	4129.9	0.419508		0.426873	
	√	—	$R_{20\text{-}21}$	4397.8	0.216624	—	0.221249	—
			$R_{19\text{-}20}$	4231.6	0.417289		0.424615	
	—	√	$R_{20\text{-}21}$	4379.2	0.216802	√	0.221431	—
			$R_{19\text{-}20}$	4379.2	0.414200		0.421472	
	√	√	$R_{20\text{-}21}$	4647.7	0.214327	√	0.218902	—
			R_{19a}	4477.4	0.412225		0.419462	

In relation to the earth overcurrent relays, miscoordination occurs due to the interconnection of DGs in various configurations, like phase overcurrent relays, as indicated in Table 8. The miscoordination cases are highlighted by the shaded cells in Table 8 where the time difference between the operation times of the backup relay and the primary relay is less than *CTI*. This issue arises because the zero-sequence path from the DGs to the fault point is closed by connecting the transformer of the DGs in a delta/star-earthed configuration, with the star-earthed side at 11 kV.

As deduced from the results, the conventional concept does not verify the coordination between relays due to the interconnection of DGs in various configurations. This problem arises from the change in the short circuit level resulting from transforming the network from a radial distribution network to a meshed distribution network. Additionally, the fault current flowing through the primary relay may differ from the fault current flowing through the backup relay by the amount of fault current that the DG contributes. Moreover, bidirectional currents become possible, which is not compatible with conventional overcurrent relays.

For fault F2, relays $R_{19\text{-}27}$ and $R_{27\text{-}30}$ detect the current injected into the fault by the Photovoltaic (PV) system in the opposite direction of normal operation. This may result in a false trip occurring, even though these relays are normally nondirectional. Moreover, this kind of tripping isolates a healthy part of the network, which is undesirable. Therefore, the use of directional overcurrent relays is necessary to ensure proper protection of the distribution system with distributed generators (DGs). However, selecting the worst condition when DGs are connected requires an extensive study to establish a general rule that can be applied to future studies, as discussed in the following section.

5. Modified Overcurrent Relays Coordination for Distribution Systems with Distributed Generation Units

As mentioned in the previous section, conventional coordination fails to ensure proper coordination between relays due to the interconnection of the DGs in various configurations. When DGs are integrated into the network, nearly every segment of the feeder necessitates two relays: a forward relay and a backward relay, to achieve comprehensive fault isolation through directional overcurrent schemes. Each backward relay is also identified by two numbers: the first number denotes the sending busbar, and the second represents the receiving busbar, as depicted in Figure 1 with dashed rectangles. For instance, in the case of feeder (1-2), $R_{1\text{-}2}$ serves as the forward relay, while $R_{2\text{-}1}$ functions as the corresponding backward relay, as shown in Figure 1. Forward relays are initially coordinated together, followed by the subsequent individual coordination of backward relays.

5.1. Coordination of Forward Relays

Inserting DGs into the network results in more constraints. The number of constraints is determined based on the possibilities of connecting and disconnecting DGs. For example, the first two constraints involve relays $R_{7\text{-}8}$ and $R_{8\text{-}10}$, using a solid three-phase fault at $R_{8\text{-}10}$ without a DG (Zct_{1a}) and with a DG connected to busbar 7 (Zct_{1b}). These constraints are treated as inequality constraints as follows:

$$Z_{CTI1a} = max\{0\ ,\ (minCTI - (t_{R7-8} - t_{R8-10}))\} \tag{12}$$

$$Z_{CTI1b} = max\{0\ ,\ (minCTI - (t_{R7-8} - t_{R8-10}))\} \tag{13}$$

where 'Zct_{1a}' represents the constraint without DG presence, and 'Zct_{1b}' represents the constraint with DG presence. The coordination between the forward relays of the entire system is achieved using this concept. Therefore, the fitness function for all forward relays in the RHS feeder is as follows:

$$fitness = \sum_{i=1}^{N} t_i + \sum_{j=1}^{11} K_j \cdot \left(Z_{CTIja} + Z_{CTIjb}\right) \tag{14}$$

where the arbitrary factor K_1 is set to 8, K_2 and K_4 are set to 4, whereas K_3, K_5, K_7, K_8, K_9, K_{10} and K_{11} are all set to 3, and K_6 is set to 3.4. Symbols '*a*' and '*b*' denote the constraint statuses under DG absence, considering the maximum jointed fault current ($I_{fmax\text{-}jointed}$), as shown in Table 3, and the constraint under DG presence, considering $I_{fmax\text{-}jointed}$, as shown in Table 9, respectively. Consequently, the number of constraints is doubled compared to those associated with conventional coordination. Symbol '*j*' refers to the number of pairs, ranging from 1 to 11, as shown in Tables 3 and 9. The maximum number of generations is set to 500, the generation gap is 0.8, the mutation rate varies based on the number of variables, and a single crossover rate is assigned in the GA. The best fitness function value is 5.8818 s. The *TDS* values verifying this optimal value are provided in Table 10. Similarly, the coordination among all forward relays in the LHS feeder is achieved by minimizing the following fitness function.

$$fitness = \sum_{i=1}^{N} t_i + \sum_{j=1}^{14} K_j \cdot \left(Z_{CTIja} + Z_{CTIjb} + Z_{CTIjc} + Z_{CTIjd} \right) \quad (15)$$

where the arbitrary factors K_1 to K_{11} and K_{13} are set to 3, while K_{12} and K_{14} are set to 2. As shown in Equation (16), each pair of relays has four constraints. This is because the LHS feeder accommodates two DGs that may be either connected or disconnected, resulting in four possible scenarios. Symbol '*a*' refers to the constraint status under DG absence, considering the maximum jointed fault current ($I_{fmax\text{-}jointed}$), as depicted in Table 5. Conversely, symbols '*b*', '*c*', and '*d*' denote the remaining three constraints associated with all possible interconnections of the two DGs, considering $I_{fmax\text{-}jointed}$, as detailed in Table 11. Symbol '*j*' represents the pair number, ranging from 1 to 14, as shown in Tables 5 and 11. The maximum number of generations is set to 600, the generation gap is 0.8, the mutation rate varies based on the number of variables, and a single crossover rate is assigned in the GA. The optimal fitness function value is 6.3013 s. The *TDSs* verifying this optimal value are provided in Table 12. Lastly, the obtained settings of the phase and earth overcurrent relays are summarized in the second part of Table 10.

Table 9. Maximum jointed fault current for each two cascaded pairs of forward relays of the RHS feeder (from $R_{8\text{-}10}$ to $R_{1\text{-}2}$) under the presence of DG connected to busbar 7.

No. of Pairs	Pair of Relays		DG status	I_{Fmax} (For Phase Faults) (A)		I_{Fmax} (For Earth Faults) (A)	
	Backup	Primary	WT	Backup	Primary	Backup	Primary
1	$R_{7\text{-}8}$	$R_{8\text{-}10}$	√	4944.7	4944.7	4387.7	4387.7
2	$R_{6\text{-}7}$	$R_{7\text{-}8}$	√	4736.77	5058.4	4369.8	4535.2
3	$R_{6\text{-}7}$	$R_{7\text{-}14}$	√	4753.02	5075.8	4391.3	4557.5
4	$R_{5\text{-}6}$	$R_{6\text{-}7}$	√	4811.4	4811.4	4472	4472
5	$R_{4\text{-}5}$	$R_{5\text{-}6}$	√	4917.6	4917.6	4621.6	4621.6
6	$R_{3\text{-}4}$	$R_{4\text{-}5}$	√	4985.4	4985.4	4719	4719
7	$R_{3\text{-}4}$	$R_{4\text{-}13}$	√	4987.35	5303.16	4722.1	4885.4
8	$R_{2\text{-}3}$	$R_{3\text{-}4}$	√	5013.5	5013.5	4760.3	4760.3
9	$R_{1\text{-}2}$	$R_{2\text{-}3}$	√	5072.9	5072.9	4848.3	4848.3
10	$R_{1\text{-}2}$	$R_{2\text{-}11}$	√	5082.16	5395.4	4863.1	5024.5
11	$R_{1\text{-}2}$	$R_{2\text{-}12}$	√	5083.06	5396.5	4864.4	5025.9

Table 10. The modified coordination results for forward relays.

Feeder	Relays	For Phase Faults		For Earth Faults	
		I_P	TDS	I_P	TDS
RHS feeder	R_{8-10}	73	0.02	15	0.02
	R_{7-8}	110	0.131	22	0.1782
	R_{7-14}	74	0.02	15	0.02
	R_{6-7}	183	0.2084	37	0.3021
	R_{5-6}	204	0.2945	41	0.4359
	R_{4-5}	240	0.368	48	0.5573
	R_{4-13}	37	0.02	8	0.02
	R_{3-4}	276	0.4356	56	0.6703
	R_{2-3}	313	0.4977	63	0.7808
	R_{2-11}	37	0.02	8	0.02
	R_{2-12}	37	0.02	8	0.02
	R_{1-2}	385	0.5354	77	0.8666
LHS feeder	R_{27-28}	37	0.02	8	0.02
	R_{27-29}	37	0.02	8	0.02
	R_{27-30}	37	0.02	8	0.02
	R_{19-27}	110	0.128	22	0.176
	R_{21-22}	22	0.02	5	0.02
	R_{20-21}	95	0.1341	19	0.1818
	R_{19-20}	168	0.2143	34	0.3072
	R_{18-19}	278	0.2641	56	0.4037
	R_{18-25}	37	0.02	8	0.02
	R_{17-18}	314	0.3332	63	0.5207
	R_{23-24}	37	0.02	8	0.02
	R_{17-23}	73	0.1452	15	0.1921
	R_{16-17}	385	0.3836	77	0.6193
	R_{15-16}	421	0.4438	85	0.7261
	R_{1-15}	458	0.5006	92	0.8324

Table 11. Maximum jointed fault current for each two cascaded pairs of forward relays of the LHS feeder (from R_{27-30} to R_{1-15}) under the presence of DG connected to busbar 7.

No. of Pairs	Pair of Relays		DGs status		I_{Fmax} (For Phase Faults) (A)		I_{Fmax} (For Earth Faults) (A)	
	Backup	Primary	WT	PV	Backup	Primary	Backup	Primary
1	R_{19-27}	R_{27-28}	√	—	4882.2	4882.2	4285.5	4285.5
			—	√	4540.3	4887.5	4123.1	4290
			√	√	4885.6	5235	4368.1	4539.6
2	R_{19-27}	R_{27-29}	√	—	4882.2	4882.2	4285.5	4285.5
			—	√	4540.3	4887.5	4123.1	4290
			√	√	4885.6	5235	4368.1	4539.6
3	R_{19-27}	R_{27-30}	√	—	4882.2	4882.2	4285.5	4285.5
			—	√	4540.5	4540.5	4123.1	4123.1
			√	√	4885.8	4885.8	4341.4	4341.4
4	R_{20-21}	R_{21-22}	√	—	4957.8	4957.8	4368.7	4368.7
			—	√	4937.1	4937.1	4350	4350
			√	√	5302.3	5302.3	4615.9	4615.9
5	R_{19-20}	R_{20-21}	√	—	4655.3	4979.6	4231.6	4397.8
			—	√	4959.1	4959.1	4379.2	4379.2
			√	√	5002.2	5326.7	4477.4	4647.7

Table 11. *Cont.*

No. of Pairs	Pair of Relays		DGs status		I_{Fmax} (For Phase Faults) (A)		I_{Fmax} (For Earth Faults) (A)	
	Backup	Primary	WT	PV	Backup	Primary	Backup	Primary
6	$R_{18\text{-}19}$	$R_{19\text{-}20}$	√	—	4703	4703	4298.7	4298.7
			—	√	4664.6	5011.4	4287.3	4453.1
			√	√	4705.6	5055	4381.1	4550.8
7	$R_{18\text{-}19}$	$R_{19\text{-}27}$	√	—	4684.9	5004.7	4276.3	4441.9
			—	√	4649.4	4649.4	4267.1	4267.1
			√	√	4688.2	5008.4	4358.5	4527.5
8	$R_{17\text{-}18}$	$R_{18\text{-}19}$	√	—	4877.8	4877.8	4543.8	4543.8
			—	√	4838.6	4838.6	4534.9	4534.9
			√	√	4881.2	4881.2	4630.6	4630.6
9	$R_{17\text{-}18}$	$R_{18\text{-}25}$	√	—	4916.2	5233	4598.2	4763.3
			—	√	4876.8	5223.7	4589.9	4754.4
			√	√	4919.4	5583.6	4686.5	5023.78
10	$R_{17\text{-}23}$	$R_{23\text{-}24}$	√	—	5023.5	5023.5	4510.4	4510.4
			—	√	5017	5017	4504.3	4504.3
			√	√	5326.3	5326.3	4725.5	4725.5
11	$R_{16\text{-}17}$	$R_{17\text{-}23}$	√	—	5027.6	5333.5	4761.5	4920.3
			—	√	4988.1	5326.7	4755.3	4913.7
			√	√	5027.5	5674	4849.6	5175.1
12	$R_{16\text{-}17}$	$R_{17\text{-}18}$	√	—	5050.2	5050.2	4792	4792
			—	√	5009.6	5009.6	4787.1	4787.1
			√	√	5053.7	5053.7	4884.2	4884.2
13	$R_{15\text{-}16}$	$R_{16\text{-}17}$	√	—	5193.9	5193.9	5009.5	5009.5
			—	√	5152.2	5152.2	5004.7	5004.7
			√	√	5197.2	5197.2	5106.1	5106.1
14	$R_{1\text{-}15}$	$R_{15\text{-}16}$	√	—	5332.5	5332.5	5223	5223
			—	√	5289.4	5289.4	5220.3	5220.3
			√	√	5335.9	5335.9	5324	5324

Table 12. The modified coordination results for backward relays.

Feeder	Relays	For Phase Faults		For Earth Faults	
		I_P	TDS	I_P	TDS
RHS feeder	$R_{2\text{-}1}$	25	0.02	5	0.02
	$R_{3\text{-}2}$	25	0.0953	5	0.1233
	$R_{4\text{-}3}$	25	0.1708	5	0.2275
	$R_{5\text{-}4}$	25	0.2463	5	0.332
	$R_{6\text{-}5}$	194	0.0644	39	0.1795
	$R_{7\text{-}6}$	187	0.0852	38	0.2271
LHS feeder	$R_{15\text{-}1}$	25	0.02	5	0.02
	$R_{16\text{-}15}$	25	0.1164	5	0.1437
	$R_{17\text{-}16}$	25	0.213	5	0.2684
	$R_{18\text{-}17}$	25	0.3099	5	0.3941
	$R_{19\text{-}18}$	25	0.4069	5	0.521
	$R_{20\text{-}19}$	164	0.1274	33	0.2911
	$R_{27\text{-}19}$	25	0.4843	5	0.6269
	$R_{30\text{-}27}$	39	0.4654	8	0.6362

In conclusion, the insertion of a DG into the network can enhance the conventional coordination between relays by augmenting the fault current at the primary relay compared to that at the backup relay. This situation arises when the DG is positioned between the primary and backup relays. However, the presence of DGs can lead to miscoordination, especially when the DG is inserted upstream or downstream of both the backup and primary relays. Furthermore, relay coordination should ensure achieving a minimum *CTI* of 0.2 s under a new worst condition, accounting for DG presence. It can be deduced that the worst condition from the DG presence perspective varies based on each pair of relays as follows: If the inserted DG is connected upstream or downstream of the required pair of relays, then the worst condition is the presence of the DG. If the inserted DG is connected between the required pair of relays, then the worst condition is the absence of the DG.

5.2. Coordination of Backward Relays

Similarly, the coordination of the backward relays is achieved in a manner like the forward relays, with the difference being that the fault current source utilized for the coordination process is solely the inserted DGs. Carrying out the procedures to coordinate both the phase and earth relays of the RHS feeder (from $R_{2\text{-}1}$ to $R_{7\text{-}6}$) and those of the LHS feeder (from $R_{15\text{-}1}$ to $R_{30\text{-}27}$) under both phase and earth faults, respectively, results in the optimal settings, as documented in Table 12. The verification that the modified coordination scheme ensures proper coordination between relays in the presence of DGs is provided in the subsequent subsection.

5.3. The Evaluation of the Modified Coordination under Opening Bus Coupler

The impact of DGs on the obtained settings of both phase and earth overcurrent relay functions utilizing the modified coordination is investigated and presented in the last two columns of Tables 7 and 8, respectively. This investigation is also conducted under the selected three faults (F1, F2, and F3), which are thoroughly described in Section 4.2. The results demonstrate that the coordination is verified under fault F1 in the RHS feeder, regardless of the status of the DG (WT). Furthermore, the coordination margin between the corresponding backup and primary relays remains greater than the *CTI* under faults F2 and F3, regardless of the status of the two DGs (PV and WT) connected to the LHS feeder. This is evident in the four cases that encompass all possible network topologies for each fault. Consequently, the security percentage of the protection system is improved from 60% to 100% based on the formula presented in [30].

6. New Communicationless Overcurrent Relays Coordination Approach for Deregulated Distribution System Considering Fault Repairing Periods

To ensure the continuity of the distribution system, a bus coupler (BC) between busbars 6 and 24 is necessary within the distribution feeder, as outlined below. In the event of a fault in the feeder, the associated overcurrent relays emit tripping signals to isolate the faulted section from both sides, based on the modified coordination procedure under DG presence discussed in the previous section. However, this can result in the isolation of healthy sections downstream of the fault. Therefore, the inclusion of the BC facilitates the continued supply of power to these healthy segments of the ring, coming from opposite directions for the upper section and in the same direction for the lower section. This objective can be achieved by closing tie switches, as in a pre-established plan typical of automated distribution systems. The alteration in current direction and magnitude within these segments during fault repair can lead to relay miscoordination. Consequently, enhancing the modified coordination approach for directional overcurrent relays becomes necessary. In other words, the newly presented contribution is an improvement over previous research that utilizes Genetic Algorithm (GA) optimization in relaying coordination. This enhancement takes into account additional constraints related to fault repairing periods resulting from the closure of the bus coupler. Additionally, the proposed coordination strategy is built on employing a single setting for each relay, negating the need for additional commu-

nication channels. As a result, all conceivable configurations are taken into account during the improved coordination process. Moreover, the selected pickup current must exceed the normal current for all these potential configurations without giving rise to insensitivity issues in the event of a fault scenario associated with any possible configuration.

6.1. The Concept of the Proposed Communicationless Overcurrent Relays Coordination

The enhanced coordination procedure is founded upon two key principles: firstly, partitioning the ring into four distinct parts as depicted in Figure 7, and secondly, subdividing the coordination process into four distinct paths to encompass all potential conditions. The ring is partitioned into four parts because all forward/reverse relays within each part are coordinated under the same scenarios. This comprehensive approach to coordination is executed through the utilization of four GA subroutines, each corresponding to one of the four paths. Within each path, a combination of both forward and backward relays is considered to account for the shifts in current direction that occur within certain sections of the ring. The initial step involves delineating the four sections, as illustrated in Figure 7, based on the proposed partitioning procedure. These sections are outlined as follows:

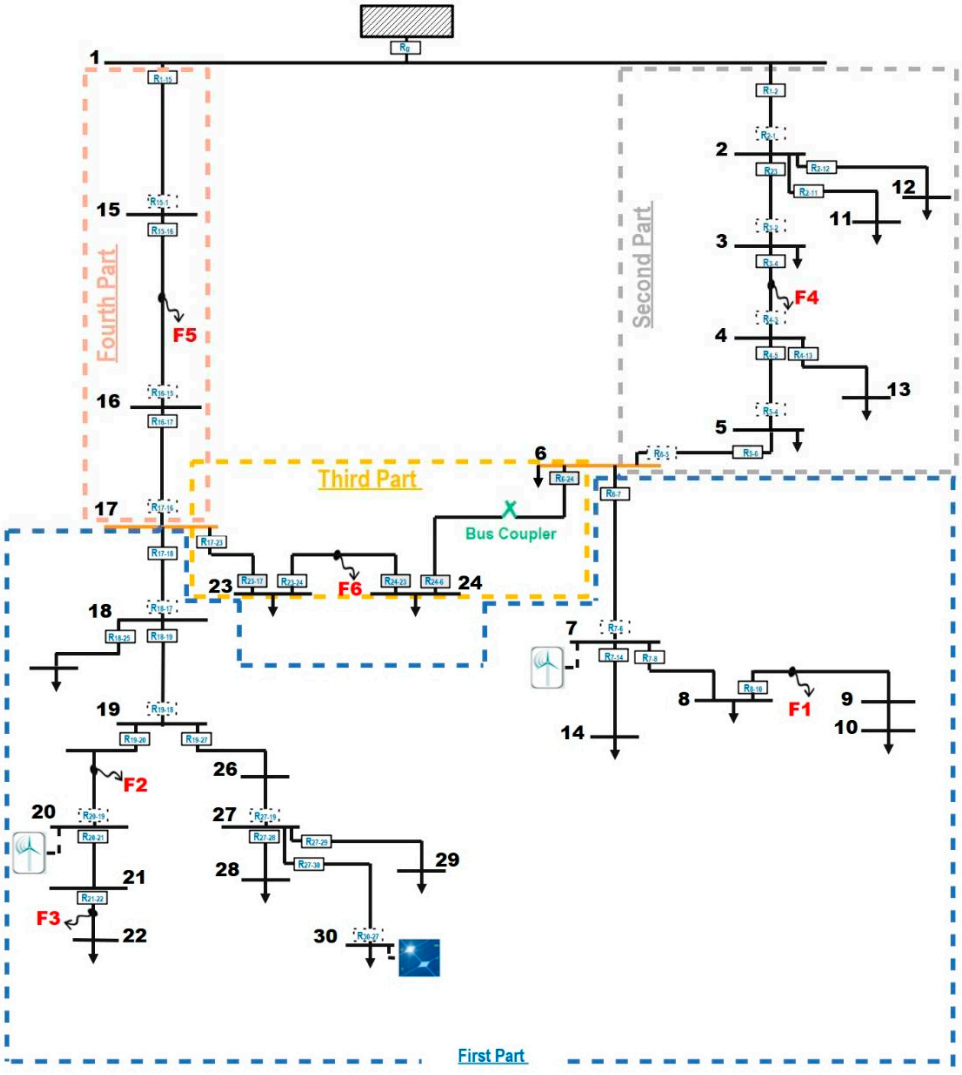

Figure 7. Actual Egyptian distribution network declaring the four parts to consider all probable conditions in the coordination process.

The 1st part consists of all the laterals branching from the ring. In simpler terms, the 1st part encompasses laterals downstream from the ring that are connected to busbars

6 and 17. The 2nd part includes all sections on the RHS of the ring, situated between the primary substation (busbar 1) and busbar 6. The 3rd part encompasses all sections located between busbars 6 and 17, which are connected to the downstream laterals. Lastly, the 4th part comprises all sections on the LHS of the ring, found between the primary substation (busbar 1) and busbar 17.

Secondly, the coordination process consists of four distinct paths, outlined as follows: The first path focuses on the relays associated with the clockwise direction of the ring, encompassing all forward relays downstream from the ring. Ensuring proper coordination within the 1st path involves verification under all potential conditions. For the forward relays in the 1st part, coordination is examined under various scenarios: connecting the bus coupler (BC) and isolating section 1-15 as a worst-case scenario (case '*a*'), connecting the BC and isolating section 1 and 2 as a worst-case scenario (case '*b*'), and opening the BC. These scenarios are presented in the nonshaded cells (from relay pair numbers 1 to 12) in Table 13. Moving to the forward relays in the 2nd part, coordination is examined under case '*a*' and the scenario of opening the BC, indicated in the shaded cells with relay symbols in Table 13. For the relays in the 3rd part, coordination is required under both case '*a*' and case '*b*' due to the presence of a DG at bus 7. These coordination scenarios are shown in the shaded cells representing relay pair numbers in Table 13. The relays in the 3rd part encompass the forward relays protecting the sections between busbar 6 and the BC, as well as the reverse relays protecting the sections between the BC and busbar 17, all while considering the clockwise direction of the ring (the first path). The coordination of the relay pair overlapping between parts 2 and 3 ($R_{5\text{-}6}$-and $R_{6\text{-}24}$) is undertaken solely under case '*a*', as presented in the shaded row of Table 13. This coordination scenario involves disconnecting the DG at busbar 7, based on conclusions drawn from the previous section to reduce computational complexity. Furthermore, the reverse relays in the 4th part are coordinated under three probable conditions due to DG presence, excluding the upstream section (section 1-15), all while considering the clockwise direction of the ring. These scenarios are displayed in the shaded cells depicting the various network topology conditions in Table 13. Consequently, the relay pair $R_{16\text{-}15}$ and $R_{15\text{-}1}$ is coordinated exclusively under the condition of opening the BC.

Similarly, the second path concerns the relays involved in the anticlockwise direction of the ring, including all forward relays downstream of the ring. The proper coordination of the involved relays in the 2nd path must be verified under all probable conditions as follows: The forward relays of the 1st part are coordinated under all three probable conditions, as illustrated in the nonshaded cells (from relay pair 1 to 12) in Table 14. The reverse relays of the 2nd part are coordinated under the three probable conditions due to the presence of DGs, except for the upstream section (section 1-2), when considering the anticlockwise direction of the ring, as illustrated in the shaded cells depicting the probable conditions of the network topology in Table 14. Therefore, the pair of relays $R_{3\text{-}2}$ and $R_{2\text{-}1}$ is coordinated under only the condition of opening BC. The involved relays of the 3rd part are the reverse relays that primarily protect the sections between busbar 6 and BC, and the forward relays that primarily protect the sections between BC and busbar 17, considering the anticlockwise direction of the ring (the second path). However, the pair of relays that overlap between parts 2 and 3 ($R_{24\text{-}6}$ and $R_{6\text{-}5}$) is only coordinated under case '*b*', as indicated in the shaded row of Table 14. Also, the pair of relays ($R_{17\text{-}23}$ and $R_{23\text{-}24}$) is coordinated under the three probable conditions by including the probable condition of opening BC. The forward relays of the 4th part are coordinated under both case '*b*' and opening BC, as illustrated in the shaded cells with relay symbols in Table 14.

Table 13. The involved relays of the 1st GA path illustrating maximum jointed fault currents under all probable conditions for each involved pair of relays.

Part No.	No. of Pairs	Pair of Relays		Network Topology					I_{Fmax} (For Phase Faults) (A)		I_{Fmax} (For Earth Faults) (A)	
				BC		DGs						
		Backup	Primary	Case a	Case b	WT (Bus 7)	WT (Bus 20)	PV	Backup	Primary	Backup	Primary
1st Part	1	R_{19-27}	R_{27-28}	√	—	√	√	—	4395.6	4395.6	3438.7	3438.7
				—	√	√	√	—	5284.9	5284.9	4515.7	4515.7
				—	—	—	√	—	4882.2	4882.2	4285.5	4285.5
	2	R_{19-27}	R_{27-29}	√	—	√	√	—	4395.6	4395.6	3438.7	3438.7
				—	√	√	√	—	5284.9	5284.9	4515.7	4515.7
				—	—	—	√	—	4882.2	4882.2	4285.5	4285.5
	3	R_{19-27}	R_{27-30}	√	—	√	√	√	4399.3	4399.3	3489.7	3489.7
				—	√	√	√	√	5287.6	5287.6	4587.8	4587.8
				—	—	—	√	√	4885.8	4885.8	4341.4	4341.4
	4	R_{20-21}	R_{21-22}	√	—	√	√	√	4780.4	4780.4	3709.7	3709.7
				—	√	√	√	√	5711.1	5711.1	4847.7	4847.7
				—	—	—	√	√	5302.3	5302.3	4615.9	4615.9
	5	R_{19-20}	R_{20-21}	√	—	√	—	√	4448.7	4448.7	3489.3	3489.3
				—	√	√	—	√	5378	5378	4621.7	4621.7
				—	—	—	—	√	4959.1	4959.1	4379.2	4379.2
	6	R_{18-19}	R_{19-20}	√	—	√	√	—	4216.3	4216.3	3403.8	3403.8
				—	√	√	√	—	5138.6	5138.6	4549.4	4549.4
				—	—	—	√	—	4703	4703	4298.7	4298.7
	7	R_{18-19}	R_{19-27}	√	—	√	—	√	4170.7	4170.7	3372.4	3372.4
				—	√	√	—	√	5082.7	5082.7	4514.6	4514.6
				—	—	—	—	√	4649.4	4649.4	4267.1	4267.1
	8	R_{17-18}	R_{18-19}	√	—	√	√	√	4393.1	4393.1	3644	3644
				—	√	√	√	√	5362.2	5362.2	4910.3	4910.3
				—	—	—	√	√	4881.2	4881.2	4630.6	4630.6
	9	R_{17-18}	R_{18-25}	√	—	√	—	—	4394.5	4394.5	3559.6	3559.6
				—	√	√	—	—	5369.2	5369.2	4804.6	4804.6
				—	—	—	—	—	4874.3	4874.3	4492.6	4492.6
	10	R_{7-8}	R_{8-10}	√	—	√	√	√	5726.4	5726.4	4873.4	4873.4
				—	√	√	√	√	5123.1	5123.1	4162.7	4162.7
				—	—	√	—	—	4944.7	4944.7	4387.7	4387.7
	11	R_{6-7}	R_{7-8}	√	—	—	√	√	5529.2	5529.2	4800.8	4800.8
				—	√	—	√	√	4908.6	4908.6	4062.1	4062.1
				—	—	—	—	—	4696.3	4696.3	4266.2	4266.2
	12	R_{6-7}	R_{7-14}	√	—	—	√	√	5551	5551	4826.7	4826.7
				—	√	—	√	√	4927.1	4927.1	4082.2	4082.2
				—	—	—	—	—	4711.4	4711.4	4286.2	4286.2
4th Part	13	R_{16-15}	R_{15-1}	—	—	—	√	√	654.8	654.8	318.1	318.1
	14	R_{17-16}	R_{16-15}	√	—	√	√	√	5018.9	5018.9	3996.1	3996.1
				—	√	√	√	√	957.4	957.4	508.1	508.1
				—	—	—	√	√	659.1	659.1	328.4	328.4

Table 13. *Cont.*

Part No.	No. of Pairs	Pair of Relays		Network Topology					I_{Fmax} (For Phase Faults) (A)		I_{Fmax} (For Earth Faults) (A)	
				BC		DGs						
		Backup	Primary	Case a	Case b	WT (Bus 7)	WT (Bus 20)	PV	Backup	Primary	Backup	Primary
3rd Part	15	$R_{23\text{-}17}$	$R_{17\text{-}16}$	√	—	√	—	—	4533.7	4533.7	3716.9	3716.9
				—	√	√	—	—	312	312	165.9	165.9
	16	$R_{23\text{-}17}$	$R_{17\text{-}18}$	√	—	√	√	√	4567.8	4567.8	3840.4	3840.4
				—	√	√	√	√	309	5581.2	172.9	5205.3
	17	$R_{24\text{-}23}$	$R_{23\text{-}17}$	√	—	√	√	√	4820.5	4820.5	4140.2	4140.2
				—	√	√	√	√	316.4	316.4	181.2	181.2
	18	$R_{6\text{-}24}$	$R_{24\text{-}23}$	√	—	√	√	√	5154.4	5154.4	4558.5	4558.5
				—	√	√	√	√	319.6	319.6	190.4	190.4
3rd-2nd	19	$R_{5\text{-}6}$	$R_{6\text{-}24}$	√	—	—	√	√	5007.8	5007.8	4578	4578
2nd Part	20	$R_{5\text{-}6}$	$R_{6\text{-}7}$	√	—	√	—	—	5019.6	5019.6	4536.8	4536.8
				—	—	√	—	—	4811.4	4811.4	4472	4472
	21	$R_{4\text{-}5}$	$R_{5\text{-}6}$	√	—	√	√	√	5176	5176	4844.2	4844.2
				—	—	√	—	—	4917.6	4917.6	4621.6	4621.6
	22	$R_{3\text{-}4}$	$R_{4\text{-}5}$	√	—	√	√	√	5247.5	5247.5	4950.6	4950.6
				—	—	√	—	—	4985.4	4985.4	4719	4719
	23	$R_{3\text{-}4}$	$R_{4\text{-}13}$	√	—	—	—	—	5165.9	5165.9	4708.9	4708.9
				—	—	—	—	—	4943.7	4943.7	4612.3	4612.3
	24	$R_{2\text{-}3}$	$R_{3\text{-}4}$	√	—	√	√	√	5277.1	5277.1	4995.8	4995.8
				—	—	√	—	—	5013.5	5013.5	4760.3	4760.3
	25	$R_{1\text{-}2}$	$R_{2\text{-}3}$	√	—	√	√	√	5339.6	5339.6	5092.1	5092.1
				—	—	√	—	—	5072.9	5072.9	4848.3	4848.3
	26	$R_{1\text{-}2}$	$R_{2\text{-}11}$	√	—	—	—	—	5264.5	5264.5	4857.4	4857.4
				—	—	—	—	—	5037.5	5037.5	4750	4750
	27	$R_{1\text{-}2}$	$R_{2\text{-}12}$	√	—	—	—	—	5265.6	5265.6	4858.8	4858.8
				—	—	—	—	—	5038.4	5038.4	4751.3	4751.3

The first and second paths related to the relays involved in the clockwise and anti-clockwise directions of the ring, including all forward relays downstream of the ring, are not sufficient due to the creation of two other paths via the existence of DGs downstream of the ring. The third and fourth paths cover these scenarios by addressing the reverse relays of the right- and left-hand-side feeder sections downstream of the ring, respectively. The remaining relays associated with cases that involve feeding upstream source side faults through distributed generation units or under power source removal must still be coordinated. Therefore, the third path is designed to achieve coordination among these remaining relays in the RHS feeder: $R_{7\text{-}6}$, $R_{6\text{-}5}$, and $R_{6\text{-}24}$. Furthermore, the fourth path is intended to achieve coordination among these remaining relays in the LHS feeder: $R_{30\text{-}27}$, $R_{27\text{-}29}$, $R_{27\text{-}28}$, $R_{27\text{-}19}$, $R_{20\text{-}19}$, $R_{19\text{-}18}$, $R_{18\text{-}25}$, $R_{18\text{-}17}$, $R_{17\text{-}23}$, and $R_{17\text{-}16}$, as introduced in the previous section. The coordination of both the third and fourth paths is achieved under different scenarios, including connecting BC and isolating section 1-15 (case '*a*'), connecting BC and isolating section 1 and 2 (case '*b*'), and opening BC.

Table 14. The involved relays of the 2nd GA path illustrating maximum jointed fault currents under all probable conditions for each involved pair of relays.

	No. of Pairs	Pair of Relays		Network Topology					I_{Fmax} (For Phase Faults) (A)		I_{Fmax} (For Earth Faults) (A)	
				BC		DGs						
		Backup	Primary	Case a	Case b	WT (B.B 7)	WT (B.B 20)	PV	Backup	Primary	Backup	Primary
1st Part	1	R_{19-27}	R_{27-28}	√	—	√	√	—	4395.6	4395.6	3438.7	3438.7
				—	√	√	√	—	5284.9	5284.9	4515.7	4515.7
				—	—	—	√	—	4882.2	4882.2	4285.5	4285.5
	2	R_{19-27}	R_{27-29}	√	—	√	√	—	4395.6	4395.6	3438.7	3438.7
				—	√	√	√	—	5284.9	5284.9	4515.7	4515.7
				—	—	—	√	—	4882.2	4882.2	4285.5	4285.5
	3	R_{19-27}	R_{27-30}	√	—	√	√	√	4399.3	4399.3	3489.7	3489.7
				—	√	√	√	√	5287.6	5287.6	4587.8	4587.8
				—	—	—	√	√	4885.8	4885.8	4341.4	4341.4
	4	R_{20-21}	R_{21-22}	√	—	√	√	√	4780.4	4780.4	3709.7	3709.7
				—	√	√	√	√	5711.1	5711.1	4847.7	4847.7
				—	—	—	√	√	5302.3	5302.3	4615.9	4615.9
	5	R_{19-20}	R_{20-21}	√	—	√	—	√	4448.7	4448.7	3489.3	3489.3
				—	√	√	—	√	5378	5378	4621.7	4621.7
				—	—	—	—	√	4959.1	4959.1	4379.2	4379.2
	6	R_{18-19}	R_{19-20}	√	—	√	√	—	4216.3	4216.3	3403.8	3403.8
				—	√	√	√	—	5138.6	5138.6	4549.4	4549.4
				—	—	—	√	—	4703	4703	4298.7	4298.7
	7	R_{18-19}	R_{19-27}	√	—	√	—	√	4170.7	4170.7	3372.4	3372.4
				—	√	√	—	√	5082.7	5082.7	4514.6	4514.6
				—	—	—	—	√	4649.4	4649.4	4267.1	4267.1
	8	R_{17-18}	R_{18-19}	√	—	√	√	√	4393.1	4393.1	3644	3644
				—	√	√	√	√	5362.2	5362.2	4910.3	4910.3
				—	—	—	√	√	4881.2	4881.2	4630.6	4630.6
	9	R_{17-18}	R_{18-25}	√	—	√	—	—	4394.5	4394.5	3559.6	3559.6
				—	√	√	—	—	5369.2	5369.2	4804.6	4804.6
				—	—	—	—	—	4874.3	4874.3	4492.6	4492.6
	10	R_{7-8}	R_{8-10}	√	—	√	√	√	5726.4	5726.4	4873.4	4873.4
				—	√	√	√	√	5123.1	5123.1	4162.7	4162.7
				—	—	√	—	—	4944.7	4944.7	4387.7	4387.7
	11	R_{6-7}	R_{7-8}	√	—	—	√	√	5529.2	5529.2	4800.8	4800.8
				—	√	—	√	√	4908.6	4908.6	4062.1	4062.1
				—	—	—	—	—	4696.3	4696.3	4266.2	4266.2
	12	R_{6-7}	R_{7-14}	√	—	—	√	√	5551	5551	4826.7	4826.7
				—	√	—	√	√	4927.1	4927.1	4082.2	4082.2
				—	—	—	—	—	4711.4	4711.4	4286.2	4286.2
2nd Part	13	R_{3-2}	R_{2-1}	—	—	√	—	—	326.4	326.4	163.8	163.8
	14	R_{3-2}	R_{2-11}	—	√	√	√	√	5011.3	5011.3	4046	4046
				√	—	√	√	√	927.5	6252.2	512.1	5609.1
				—	—	√	—	—	326.7	5395.4	167	5024.5
	15	R_{3-2}	R_{2-12}	—	√	√	√	√	5012.4	5012.4	4047.2	4047.2
				√	—	√	√	√	927.9	6253.7	512.2	5610.9
				—	—	√	—	—	326.8	5396.5	167	5025.9
	16	R_{4-3}	R_{3-2}	—	√	√	√	√	5091.1	5091.1	4129.5	4129.5
				√	—	√	√	√	933.2	933.2	519.2	519.2
				—	—	√	—	—	327.8	327.8	169.2	169.2
	17	R_{5-4}	R_{4-3}	—	√	√	√	√	5133.3	5133.3	4174.3	4174.3
				√	—	√	√	√	935.3	935.3	522.7	522.7
				—	—	√	—	—	328	328	170.4	170.4
	18	R_{5-4}	R_{4-13}	—	√	√	√	√	5127.2	5127.2	4168	4168
				√	—	√	√	√	932.5	6161.6	521.6	5459.2
				—	—	√	—	—	327.2	5303.2	170.2	4885.43
	19	R_{6-5}	R_{5-4}	—	√	√	√	√	5199.4	5199.4	4245.5	4245.5
				√	—	√	√	√	938.7	938.7	528.3	528.3
				—	—	√	—	—	328.4	328.4	172.2	172.2

Table 14. *Cont.*

	No. of Pairs	Pair of Relays		Network Topology					I_{Fmax} (For Phase Faults) (A)		I_{Fmax} (For Earth Faults) (A)	
				BC		DGs						
		Backup	Primary	Case a	Case b	WT (B.B 7)	WT (B.B 20)	PV	Backup	Primary	Backup	Primary
2nd-3rd	20	R_{24-6}	R_{6-5}	—	√	—	√	√	4989.4	4989.4	4152.3	4152.3
3rd Part	21	R_{24-6}	R_{6-7}	—	√	√	√	√	5037.9	5037.9	4245	4245
				√	—	√	√	√	620.6	5677.3	355.7	5018.4
	22	R_{23-24}	R_{24-6}	—	√	√	√	√	5193.4	5193.4	4430.1	4430.1
				√	—	√	√	√	627.4	627.4	364.9	364.9
	23	R_{17-23}	R_{23-24}	—	√	√	√	√	5541.5	5541.5	4863.8	4863.8
				√	—	√	√	√	635.3	635.3	381.1	381.1
				—	—	—	√	√	5326.3	5326.3	4725.5	4725.5
4th Part	24	R_{16-17}	R_{17-23}	—	√	√	—	—	5222.2	5222.2	4841.5	4841.5
				—	—	—	—	—	4984.9	4984.9	4655.7	4655.7
	25	R_{16-17}	R_{17-18}	—	√	—	√	√	5242.2	5242.2	4956.7	4956.7
				—	—	—	√	√	5053.7	5053.7	4884.2	4884.2
	26	R_{15-16}	R_{16-17}	—	√	√	√	√	5439.6	5439.6	5276.5	5276.5
				—	—	—	√	√	5197.2	5197.2	5106.1	5106.1
	27	R_{1-15}	R_{15-16}	—	√	√	√	√	5584.8	5584.8	5509.5	5509.5
				—	—	—	√	√	5335.9	5335.9	5324	5324

The potential insensitivity of relays involved in the 3rd part, due to the utilization of nonadaptive pickup current (single pickup current) for each relay, is addressed as follows. If a relay in the 3rd part detects a substantial current in its reverse direction, which remains below the corresponding pickup current, and subsequently the current direction changes, this indicates the connection of the bus coupler and signifies a fault in the 3rd part that is solely fed by DG/s in this direction. Consequently, all relays with the same status must be automatically adjusted to the same current multiplier setting ratio (fault current/pickup current) to uphold the security aspect of the protection system and, simultaneously, to ensure more than one to maintain sensitivity. This ratio is set to a significant value (representing the worst condition) to maintain the maximum speed of the proposed protection system.

6.2. Procedure for New Coordination Approach Computation

The GA is used to validate the optimal coordination margins by minimizing the objective function, which is the sum of operating times of the relays under the worst conditions across all network topologies. Taking into account the fault repair periods (BC status), in addition to the status of DGs in the network, results in more constraints, as shown in Tables 13 and 14 for the 1st and 2nd GA subroutines, respectively. Similarly, the relay pairs involved in the 3rd and 4th GA subroutines are examined under both case '*a*', case '*b*', and when BC is open.

For instance, in the 1st GA subroutine, every pair of relays is coordinated based on the maximum joint fault current for each two cascaded relays, taking into account the BC status and the worst DGs' condition, as presented in Table 13. Consequently, the fitness function of the 1st GA subroutine is as follows:

$$\begin{aligned} fitness = \sum_{i=1}^{N} t_i \\ &+ \sum_{j=1}^{12} K_j \cdot \left(Z_{CTIj\alpha} + Z_{CTIj\beta} + Z_{CTIj\gamma}\right) + K_{13} \cdot Z_{CTI13\gamma} \\ &+ K_{14} \cdot \left(Z_{CTI14\alpha} + Z_{CTI14\beta} + Z_{CTI14\gamma}\right) \\ &+ \sum_{j=15}^{18} K_j \cdot \left(Z_{CTIj\alpha} + Z_{CTIj\beta}\right) + K_{19} \cdot Z_{CTI19\alpha} + \sum_{j=20}^{27} K_j \cdot \left(Z_{CTIj\alpha} + Z_{CTIj\gamma}\right) \end{aligned} \quad (16)$$

where α, β, and γ correspond to the bus coupler status as shown in Table 13, while the worst condition of DGs' presence is determined based on the conclusions obtained in the previous section.

Likewise, in the 2nd GA subroutine, Table 14 displays pairs of relays for coordinating the 2nd GA path based on the maximum joint fault current for each two cascaded relays, while considering the BC status and the worst DGs' condition. Consequently, the fitness function of the 2nd GA subroutine is as follows:

$$\begin{aligned} fitness = \sum_{i=1}^{N} t_i \\ &+ \sum_{j=1}^{12} K_j \cdot \left(Z_{CTIj\alpha} + Z_{CTIj\beta} + Z_{CTIj\gamma}\right) \\ &+ K_{13} \cdot Z_{CTI13\gamma} \\ &+ \sum_{j=14}^{19} K_j \cdot \left(Z_{CTIj\alpha} + Z_{CTIj\beta} + Z_{CTIj\gamma}\right) \\ &+ K_{20} \cdot Z_{CTI20\beta} + \sum_{j=21}^{22} K_j \cdot \left(Z_{CTIj\alpha} + Z_{CTIj\beta}\right) \\ &+ K_{23} \cdot \left(Z_{CTI23\alpha} + Z_{CTI23\beta} + Z_{CTI23\gamma}\right) \\ &+ \sum_{j=24}^{27} K_j \cdot \left(Z_{CTIj\beta} + Z_{CTIj\gamma}\right) \end{aligned} \quad (17)$$

The fitness function of the third GA subroutine is as follows:

$$fitness = \sum_{i=1}^{N} t_i + \sum_{j=1}^{2} K_j \cdot \left(Z_{CTIj\alpha} + Z_{CTIj\beta} + Z_{CTIj\gamma}\right) \quad (18)$$

The fitness function of fourth GA subroutine is as follows:

$$fitness = \sum_{i=1}^{N} t_i + \sum_{j=1}^{9} K_j \cdot \left(Z_{CTIj\alpha} + Z_{CTIj\beta} + Z_{CTIj\gamma}\right) \quad (19)$$

The optimal settings of all relays that satisfy the four fitness functions across the four subroutines are determined. These settings are presented in Table 15. The arbitrary factors that satisfy all four fitness functions are as follows. At first, the arbitrary factors for the 1st fitness function are selected to guarantee achieving of the coordination constraint by making its expression significant in the formula of fitness function as follows: K_1, K_2, K_3, K_7, K_9, K_{11}, K_{12}, K_{15}, K_{20}, K_{22}, K_{23}, K_{24}, K_{25}, K_{26}, and K_{27} are set to 2, K_4, K_5, K_6, K_8, K_{13}, K_{14}, K_{16}, K_{17}, and K_{18} are set to 10, K_{10} is set to 6, and K_{19} and K_{21} are equal to 8. Secondly, the arbitrary factors for the 2nd fitness function are as follows: K_1, K_2, K_4, K_5, K_6, K_{10}, K_{16}, K_{25}, and K_{26} are set to 6, K_3 and K_{24} are equal to 8, K_7, K_8, K_9, and K_{18} are set to 10, K_{11}, K_{12} K_{19}, K_{20}, K_{22}, and K_{27} are set to 3, K_{13} and K_{21} are set to 4, K_{14}, K_{15}, and K_{23} are set to 2, and K_{17} is set to 7. Thirdly, the arbitrary factors for the 3rd fitness function are as follows: K_1 is set to 8, whereas K_2 is set to 2. Fourthly, the arbitrary factors for the 4th fitness function are as follows: K_1, K_4, K_5, K_7, K_8, and K_9 are set to 1, K_2 is set to 30, K_3 is set to 10, and K_6 is set to 3. The best values of the 1st, 2nd, 3rd, and 4th fitness functions are set to 17.4318, 14.364, 1.648, and 79.5502 s, respectively. The *TDS* values that validate this optimal value are listed in Table 15. Additionally, the corresponding *TDS* values for earth-fault relays are calculated using line-to-ground faults, as illustrated in Table 15. Ultimately, the settings for both the I_{PS} and *TDSs* of both the phase and earth OC relays are presented in Table 15.

Table 15. Proposed overcurrent relays coordination results considering fault repairing periods.

Relays	For Phase Faults		For Earth Faults	
	I_P (A)	TDS	I_P (A)	TDS
R_{27-28}	38	0.02	8	0.02
R_{27-29}	38	0.02	8	0.02
R_{27-30}	38	0.02	8	0.02
R_{21-22}	23	0.02	5	0.02
R_{20-21}	99	0.1352	20	0.1816
R_{19-20}	174	0.2169	35	0.3085
R_{19-27}	114	0.1293	23	0.1761
R_{18-19}	287	0.2688	58	0.4053
R_{18-25}	38	0.02	8	0.02
R_{17-18}	325	0.3394	65	0.5235
R_{8-10}	75	0.02	15	0.02
R_{7-8}	113	0.1347	23	0.18
R_{7-14}	75	0.02	15	0.02
R_{6-7}	187	0.2168	38	0.3074
R_{15-1}	25	0.02	5	0.02
R_{16-15}	38	0.1011	8	0.1271
R_{17-16}	75	0.2117	15	0.2824
R_{23-17}	399	0.3838	80	0.6116
R_{24-23}	435	0.4406	87	0.7129
R_{6-24}	472	0.4956	95	0.8115
R_{5-6}	678	0.4764	136	0.8381
R_{4-5}	715	0.5214	143	0.9302
R_{4-13}	38	0.02	8	0.02
R_{3-4}	752	0.5645	151	1.0189
R_{2-3}	789	0.6057	158	1.1074
R_{2-11}	38	0.02	8	0.02
R_{2-12}	38	0.02	8	0.02
R_{1-2}	864	0.6294	173	1.1791
R_{2-1}	25	0.02	5	0.02
R_{3-2}	75	0.1423	15	0.1871
R_{4-3}	112	0.2416	23	0.3284
R_{5-4}	149	0.3277	30	0.459
R_{6-5}	194	0.3997	39	0.574
R_{24-6}	393	0.3851	79	0.6015
R_{23-24}	430	0.4443	86	0.7055
R_{17-23}	466	0.5025	94	0.8067
R_{16-17}	783	0.4478	157	0.7994
R_{15-16}	820	0.492	164	0.8918
R_{1-15}	856	0.5354	172	0.98193
R_{18-17}	25	5.3177	5	2.6573
R_{19-18}	25	5.4147	5	2.7886
R_{20-19}	174	1.325	35	1.3526
R_{27-19}	25	5.4921	5	2.8985
R_{30-27}	41	4.5056	9	2.5215
R_{7-6}	195	0.4108	39	1.8708

7. New Protection Coordination Approach Evaluation

The proposed approach is tested against faults associated with normal configuration, DGs' presence, and connecting the BC to the selected distribution network under various three-phase and earth faults, as indicated in Tables 16 and 17. The performance of the proposed approach is evaluated as follows.

Table 16. The performance of the proposed overcurrent relays coordination under three-phase faults considering samples of all possible network topologies.

Fault	Network Topology	Relay	I_F (A)	Operating Time (s)	Miscoordination	Insensitivity
F_4	Normal operation	R_{3-4}	4969.5	2.053314	—	—
		R_{2-3}	4969.5	2.261769		
	DGs inserted	R_{3-4}	5013.5	2.043592	—	—
		R_{2-3}	5013.5	2.250787		
		R_{4-3}	327.89	1.557657	—	—
		R_{5-4}	327.89	2.885769		
	Section 1-2 disconnected	R_{4-3}	5115.7	0.42587	—	—
		R_{5-4}	5115.7	0.626103		
	Section 1-15 disconnected	R_{3-4}	5277.1	1.98882	—	—
		R_{2-3}	5277.1	2.188967		
		R_{4-3}	934.5	0.780423	—	—
		R_{5-4}	934.5	1.226689		
F_5	Normal operation	R_{15-16}	5286.9	1.813728	—	—
		R_{1-15}	5286.9	2.021169		
	DGs inserted	R_{15-16}	5335.9	1.804626	—	—
		R_{1-15}	5335.9	2.010793		
		R_{16-15}	656.6	0.241257	—	—
		R_{17-16}	656.6	0.66829		
	Section 1-2 disconnected	R_{15-16}	5584.8	1.760933	—	—
		R_{1-15}	5584.8	1.961014		
		R_{16-15}	951.2	0.21269	—	—
		R_{17-16}	951.2	0.568651		
	Section 1-15 disconnected	R_{16-15}	4910.07	0.138558	—	—
		R_{17-16}	4910.07	0.339761		
F_6	Normal operation	R_{23-24}	4710.7	1.268375	—	—
		R_{17-23}	4710.7	1.485582		
	DGs inserted	R_{23-24}	5326.3	1.204981	—	—
		R_{17-23}	5326.3	1.408942		
	Section 1-2 disconnected	R_{23-24}	5541.5	1.185836	—	—
		R_{17-23}	5541.5	1.385848		
		R_{24-23}	317.62	1.6171	—	—
		R_{6-24}	317.62	1.8189		
		R_{7-6}	317.62	5.865651		
	Section 1-15 disconnected	R_{23-24}	635.3	7.937178	—	—
		R_{17-23}	635.3	11.314869		
		R_{24-23}	4944.91	1.238169	—	—
		R_{6-24}	4944.91	1.442524		

Consider a solid three-phase fault (F_4) at relay R_{3-4}, simulated in section 3-4. The potential network topologies are as follows:

- Under faults associated with normal configuration, the operating time (t_{op}) of relay R_{2-3} is greater than that of relay R_{3-4} by a difference equal to or greater than *CTI*, as shown in Table 16.
- With the insertion of DGs, the t_{op} of relay R_{2-3} is greater than that of relay R_{3-4} by a difference equal to or greater than *CTI*. Additionally, the t_{op} of backward relay R_{5-4} is greater than that of relay R_{4-3} by a difference equal to or greater than *CTI*, as shown in Table 16.
- With section 1-2 disconnected, the BC connected, and DGs connected, the t_{op} of relay R_{5-4} is greater than that of relay R_{4-3} by a difference equal to or greater than *CTI*, as shown in Table 16.

- With section 1-15 disconnected, BC connected, and DGs connected, the t_{op} of relay $R_{2\text{-}3}$ is greater than that of relay $R_{3\text{-}4}$ by a difference equal to or greater than *CTI*. Simultaneously, the t_{op} of backward relay $R_{5\text{-}4}$ is greater than that of relay $R_{4\text{-}3}$ by a difference equal to or greater than *CTI*, as shown in Table 16.

Table 17. The performance of the proposed overcurrent relays coordination under earth faults considering samples of all possible network topologies.

Fault	Network Topology	Relay	I_F (A)	Operating Time (s)	Miscoordination	Insensitivity
F_4	Normal operation	$R_{3\text{-}4}$	4649.3	2.010589	—	—
		$R_{2\text{-}3}$	4649.3	2.215555		
	DGs inserted	$R_{3\text{-}4}$	4760.3	1.996366	—	—
		$R_{2\text{-}3}$	4760.3	2.19968		
	Section 1-2 disconnected	$R_{4\text{-}3}$	169.92	1.126661	—	—
		$R_{5\text{-}4}$	169.92	1.820858		
		$R_{4\text{-}3}$	4155.8	0.419762	—	—
		$R_{5\text{-}4}$	4155.8	0.619982		
	Section 1-15 disconnected	$R_{3\text{-}4}$	4995.8	1.967854	—	—
		$R_{2\text{-}3}$	4995.8	2.167867		
		$R_{4\text{-}3}$	521.3	0.71385	—	—
		$R_{5\text{-}4}$	521.3	1.093519		
F_5	Normal operation	$R_{15\text{-}16}$	5106.7	1.753821	—	—
		$R_{1\text{-}15}$	5106.7	1.959139		
	DGs inserted	$R_{15\text{-}16}$	5324	1.73209	—	—
		$R_{1\text{-}15}$	5324	1.934539		
	Section 1-2 disconnected	$R_{16\text{-}15}$	322.54	0.231881	—	—
		$R_{17\text{-}16}$	322.54	0.624726		
		$R_{15\text{-}16}$	5509.5	1.714616	—	—
		$R_{1\text{-}15}$	5509.5	1.914763		
	Section 1-15 disconnected	$R_{16\text{-}15}$	499.03	0.206481	—	—
		$R_{17\text{-}16}$	499.03	0.544519		
		$R_{16\text{-}15}$	3887.14	0.135111	—	—
		$R_{17\text{-}16}$	3887.14	0.336305		
F_6	Normal operation	$R_{23\text{-}24}$	4284.5	1.214815	—	—
		$R_{17\text{-}23}$	4284.5	1.422703		
	DGs inserted	$R_{23\text{-}24}$	4725.5	1.183933	—	—
		$R_{17\text{-}23}$	4725.5	1.385748		
	Section 1-2 disconnected	$R_{23\text{-}24}$	4863.8	1.175126	—	—
		$R_{17\text{-}23}$	4863.8	1.375216		
		$R_{24\text{-}23}$	185.27	6.551969	—	—
		$R_{6\text{-}24}$	185.27	8.447862		
	Section 1-15 disconnected	$R_{23\text{-}24}$	381.1	3.268152	—	—
		$R_{17\text{-}23}$	381.1	3.977966		
		$R_{24\text{-}23}$	4293.5	1.230654	—	—
		$R_{6\text{-}24}$	4293.5	1.434478		

Likewise, consider a solid three-phase fault (F_5) at relay $R_{15\text{-}16}$ (section 15-16). The potential network topologies are as follows:

- In faults associated with normal configuration, the t_{op} of relay $R_{1\text{-}15}$ is greater than that of relay $R_{15\text{-}16}$ by a difference equal to or greater than *CTI*, as shown in Table 16.
- With the insertion of DGs, the t_{op} of relay $R_{1\text{-}15}$ is greater than that of relay $R_{15\text{-}16}$ by a difference equal to or greater than *CTI*. Simultaneously, the t_{op} of backward relay $R_{17\text{-}16}$ is greater than that of relay $R_{16\text{-}15}$ by a difference equal to or greater than *CTI*, as shown in Table 16.
- With section 1-2 disconnected, BC connected, and DGs connected, the t_{op} of relay $R_{1\text{-}15}$ is greater than that of relay $R_{15\text{-}16}$ by a difference equal to or greater than *CTI*.

Simultaneously, the t_{op} of backward relay $R_{17\text{-}16}$ is greater than that of relay $R_{16\text{-}15}$ by a difference equal to or greater than *CTI*, as shown in Table 16.

- With section 1-15 disconnected, BC connected, and DGs connected, the t_{op} of relay $R_{17\text{-}16}$ is greater than that of relay $R_{16\text{-}15}$ by a difference equal to or greater than *CTI*, as shown in Table 16.

Furthermore, consider a solid three-phase fault (F_6) at relay $R_{23\text{-}24}$ (section 23-24). The potential network topologies are as follows:

- In faults associated with normal configuration, the t_{op} of relay $R_{17\text{-}23}$ is greater than that of relay $R_{23\text{-}24}$ by a difference equal to or greater than *CTI*, as shown in Table 16.
- With the insertion of DGs, the t_{op} of relay $R_{17\text{-}23}$ is greater than that of relay $R_{23\text{-}24}$ by a difference equal to or greater than *CTI*, as shown in Table 16.
- When section 1-2 is disconnected, the BC is connected, and DGs are connected, the t_{op} of Relay $R_{17\text{-}23}$ is more than that of relay $R_{23\text{-}24}$ by a difference equal to or more than *CTI* On the other hand, the backward relays did not sense the fault current because the fault current value is lower than the corresponding pickup currents at these relays. This insensitivity problem is overcome by the presented idea illustrated in the previous section where the relays $R_{23\text{-}24}$ and $R_{6\text{-}24}$ sense this fault F6 and then the ratio of current multiplier setting is activated to be 6.5. As declared in the shaded cells in Table 16, the t_{op} of relay $R_{23\text{-}24}$ is more than that of relay $R_{6\text{-}24}$ by a difference equal to or more than *CTI*. Fortunately, the remote backup relay $R_{7\text{-}6}$ senses the fault and clears it under the failure case of both the primary and the local backup relays.
- With section 1-2 disconnected, BC connected, and DGs connected, the t_{op} of Relay $R_{17\text{-}23}$ is greater than that of relay $R_{23\text{-}24}$ by a difference equal to or greater than *CTI*. However, the backward relays did not detect the fault current as it was lower than the corresponding pickup currents for these relays. This insensitivity issue is resolved through the presented concept outlined in the previous section, where relays $R_{23\text{-}24}$ and $R_{6\text{-}24}$ detect this fault F6 and then activate a current multiplier setting ratio of 6.5. As indicated in the shaded cells of Table 16, the t_{op} of relay $R_{23\text{-}24}$ is greater than that of relay $R_{6\text{-}24}$ by a difference equal to or greater than *CTI*. Fortunately, the remote backup relay $R_{7\text{-}6}$ detects the fault and clears it in the event of failure of both the primary and local backup relays.
- With section 1-15 disconnected, BC connected, and DGs connected, the t_{op} of relay $R_{17\text{-}23}$ is greater than that of relay $R_{23\text{-}24}$ by a difference equal to or greater than *CTI*. Simultaneously, the t_{op} of backward relay $R_{6\text{-}24}$ is greater than that of relay $R_{24\text{-}23}$ by a difference equal to or greater than *CTI*, as shown in Table 16.

With respect to the earth overcurrent relays, the coordination scheme is suitable for all possible configurations, just like the phase overcurrent relays, as indicated in Table 17.

8. Conclusions

This paper introduces a dependable communicationless approach to coordinating overcurrent relays within an actual Egyptian distribution system, while considering various potential operating conditions during both fault repair periods and the presence of DGs. The study encompasses the determination of optimal types, sizes, and placements of DGs to fulfill the objective of minimizing energy costs and environmental impact. Incorporating renewable energy sources as distributed generators (DGs) has reduced carbon dioxide emissions and mitigates global warming. Allocating DGs to cover just 33% of the load demand leads to a 14.8% reduction in energy costs, along with a 33.8% decrease in carbon dioxide emissions and a 54.4% reduction in power loss. Through extensive investigation, the impact of DG connections on coordination concepts is explored. The findings suggest that the most critical DG scenario depends on the DG's location relative to the considered relay pair. Specifically, if the inserted DG is connected upstream or downstream of the relay pair, the worst condition is when the DG is present; conversely, if the DG is connected between the relay pair, the worst condition arises when the DG is absent. Furthermore, the presented communicationless coordination approach demonstrates its reliability during

fault repair periods (including bus coupler connections) both in the absence and presence of DGs. This reliability is achieved by considering all four potential fault paths that may occur. The first and second paths pertain to relays associated with the clockwise and anticlockwise directions of the ring, encompassing all relays downstream from the ring, respectively. The third and fourth paths, created due to the presence of DGs, concern reverse relays situated in the right-hand- and left-hand-side feeder sections that lie downstream from the ring, respectively.

The proposed coordination is established by utilizing a singular setting for each relay, thereby eliminating the necessity for additional communication channels. This coordination is achieved through the consideration of load flow across all potential conditions. Furthermore, a novel solution is introduced to address the potential insensitivity issue concerning relays linked to the sections connecting the right- and left-hand-side feeders during fault repair periods in the presence of DGs. In conclusion, the results provide compelling evidence for the reliability of the proposed coordination approach across a spectrum of potential system configurations and fault scenarios.

Author Contributions: Conceptualization, M.A.E.; Data curation, A.M.A.E.A.; Formal analysis, A.F.Z., H.A.K., A.M.A.E.A. and T.F.; Investigation, M.A.E.; Methodology, M.A.E., A.F.Z. and T.F.; Software, M.A.E., A.M.A.E.A. and T.F.; Validation, H.A.K.; Writing—original draft, M.A.E.; Writing—review & editing, A.F.Z. All authors have read and agreed to the published version of the manuscript.

Funding: This research received no external funding.

Data Availability Statement: Data are contained within the article.

Conflicts of Interest: The authors declare no conflict of interest.

Appendix A

The cable and load data of the simulated 11 kV primary distribution network located in Sadat City, Menoufia, Egypt, are listed in Tables A1 and A2, respectively, as follows:

Table A1. The data of cables of the 11 kV primary distribution network.

Armored Aluminum Conductor					
Section	**Cross Section**	**Current Rating In Ground at 25 °C (Amp)**	**Resistance 50 Hz at 90 °C (Ω\Km)**	**Reactance at 50 Hz (Ω\Km)**	**Capacitance B (mhos/km) × 10^{-6}**
1-2	3 × (1 × 240)	374	0.161	0.099	153.938
2-11	3 × 240	342	0.161	0.089	150.79645
2-12	3 × 240	342	0.161	0.089	150.79645
2-3	3 × (1 × 240)	374	0.161	0.099	153.938
3-4	3 × 240	342	0.161	0.089	150.79645
4-5	3 × (1 × 240)	374	0.161	0.099	153.938
4-13	3 × 240	342	0.161	0.089	150.79645
5-6	3 × (1 × 240)	374	0.161	0.099	153.938
6-7	3 × (1 × 240)	374	0.161	0.099	153.938
6-24	3 × (1 × 240)	374	0.161	0.099	153.938
7-8	3 × (1 × 240)	374	0.161	0.099	153.938
8-9	3 × (1 × 240)	374	0.161	0.099	153.938
9-10	3 × 150	270	0.265	0.094	125.66371
7-14	3 × 70	176	0.568	0.106	94.24778
1-15	3 × (1 × 240)	374	0.161	0.099	153.938
15-16	3 × (1 × 240)	374	0.161	0.099	153.938
16-17	3 × (1 × 240)	374	0.161	0.099	153.938
17-18	3 × (1 × 240)	374	0.161	0.099	153.938
17-23	3 × (1 × 240)	374	0.161	0.099	153.938
23-24	3 × (1 × 240)	374	0.161	0.099	153.938
18-19	3 × (1 × 240)	374	0.161	0.099	153.938
18-25	3 × 70	176	0.568	0.106	94.24778
19-20	3 × 70	176	0.568	0.106	94.24778
20-21	3 × (1 × 240)	374	0.161	0.099	153.938
21-22	3 × 70	176	0.568	0.106	94.24778
19-26	3 × (1 × 240)	374	0.161	0.099	153.938
26-27	3 × 240	342	0.161	0.089	150.79645
27-28	3 × 70	176	0.568	0.106	94.24778
27-29	3 × 70	176	0.568	0.106	94.24778
27-30	3 × 70	176	0.568	0.106	94.24778

Table A2. The data of loads of the 11 kV primary distribution network.

Busbar Number	Active Power (MW)	Reactive Power (MVAR)
12	0.4125	0.363790805
11	0.44	0.33
3	0.4235	0.350924137
13	0.3905	0.387310922
5	0.451	0.314799936
6	0.297	0.143843665
24	0.4675	0.289730478
23	0.396	0.381685735
14	0.847	0.701848274
8	0.4125	0.363790805
10	0.825	0.727581611
29	0.429	0.344178733
28	0.4345	0.337208763
30	0.4455	0.322536432
20	0.88	0.66
21	0.902	0.629599873
22	0.297	0.143843665
25	0.4235	0.350924137
16	0.44	0.33
15	0.44	0.33

References

1. Esmail, E.; Elgamasy, M.; Elkalashy, N.; Elsadd, M. Detection and experimental investigation of open conductor and single-phase earth return faults in distribution systems. *Int. J. Electr. Power Energy Syst.* **2022**, *140*, 1080–1089. [CrossRef]
2. Gómez-Luna, E.; Candelo-Becerra, J.; Vasquez, J. A New Digital Twins-Based Overcurrent Protection Scheme for Distributed Energy Resources Integrated Distribution Networks. *Energies* **2023**, *16*, 5545. [CrossRef]
3. Guerraiche, K.; Dekhici, L.; Chatelet, E.; Zeblah, A. Techno-Economic Green Optimization of Electrical Microgrid Using Swarm Metaheuristics. *Energies* **2023**, *16*, 1803. [CrossRef]
4. Tavarov, S.S.; Sidorov, A.; Čonka, Z.; Safaraliev, M.; Matrenin, P.; Senyuk, M.; Beryozkina, S.; Zicmane, I. Control of Operational Modes of an Urban Distribution Grid under Conditions of Uncertainty. *Energies* **2023**, *16*, 3497. [CrossRef]
5. Nadeem, T.B.; Siddiqui, M.; Khalid, M.; Asif, M. Distributed energy systems: A review of classification, technologies, applications, and policies. *Energy Strategy Rev.* **2023**, *48*, 101096. [CrossRef]
6. Electric Power Research Institute Webpage. April 2008. Available online: https://www.epri.com/gg/newgen/disgen/index.html (accessed on 20 July 2023).
7. Gas Research Institute. *Distributed Power Generation: A Strategy for a Competitive Energy Industry*; Gas Research Institute: Chicago, IL, USA, 1998.
8. Nogueira, W.C.; Garcés Negrete, L.P.; López-Lezama, J.M. Optimal Allocation and Sizing of Distributed Generation Using Interval Power Flow. *Sustainability* **2023**, *15*, 5171. [CrossRef]
9. Majeed, A.A.; Altaie, A.S.; Abderrahim, M.; Alkhazraji, A. A Review of Protection Schemes for Electrical Distribution Networks with Green Distributed Generation. *Energies* **2023**, *16*, 7587. [CrossRef]
10. Sharaf, H.M.; Zeineldin, H.H.; Ibrahim, D.K.; EL-Zahab, E.E.A. A proposed coordination strategy for meshed distribution systems with DG considering user-defined characteristics of directional inverse time overcurrent relays. *Int. J. Electr. Power Energy Syst.* **2015**, *65*, 49–58. [CrossRef]
11. Zeineldin, H.H.; Mohamed, Y.A.-R.I.; Khadkikar, V.; Pandi, V.R. A protection coordination index for evaluating distributed generation. impacts on protection for meshed distribution systems. *IEEE Trans. Smart Grid* **2013**, *4*, 1523–1532. [CrossRef]
12. Tjahjono, A.; Anggriawan, D.; Faizin, A.; Priyadi, A.; Pujiantara, M.; Taufik, T.; Purnomo, M. Adaptive modified firefly algorithm for optimal coordination of overcurrent relays. *IET Gener. Transm. Distrib.* **2017**, *11*, 2575–2585. [CrossRef]
13. Lim, S.; Kim, J.; Kim, M.; Kim, J. Improvement of protection coordination of protective devices through application of a SFCL in a power distribution system with a dispersed generation. *IEEE Trans. Appl. Supercond.* **2012**, *22*, 5601004.
14. Kim, Y.; Jo, H.; Joo, S. Analysis of impacts of superconducting fault current limiter (SFCL) placement on distributed generation (DG) expansion. *IEEE Trans. Appl. Supercond.* **2016**, *26*, 5602305. [CrossRef]
15. Ibrahim, D.K.; EL-Zahab, E.E.A.; Mostafa, S.A. New coordination approach to minimize the number of re-adjusted relays when adding DGs in interconnected power systems with a minimum value of fault current limiter. *Int. J. Electr. Power Energy Syst.* **2017**, *85*, 32–41. [CrossRef]
16. Shih, M.Y.; Conde, A.; Leonowicz, Z.; Martirano, L. An adaptive overcurrent coordination scheme to improve relay sensitivity and overcome drawbacks due to distributed generation in smart grids. *IEEE Trans. Ind. Appl.* **2017**, *53*, 5217–5228. [CrossRef]

17. Wan, H.; Li, K.; Wong, K. An multi-agent approach to protection relay coordination with distributed generators in industrial power distribution system. In Proceedings of the Fourtieth IAS Annual Meeting. Conference Record of the 2005 Industry Application Conference, Hong Kong, China, 2–6 October 2005; Volume 2, pp. 830–836.
18. Elsadd, M.A.; Kawady, T.A.; Taalab, A.M.I.; Elkalashy, N.I. Adaptive optimum coordination of overcurrent relays for deregulated distribution system considering parallel feeders. *Electr. Eng.* **2021**, *103*, 1849–1867. [CrossRef]
19. Khalifa, L.S.; Elsadd, M.A.; Abd El-Aal, R.A.; El-Makkawy, S.M. Enhancing Recloser-Fuse Coordination Using Distributed Agents in Deregulated Distribution Systems. In Proceedings of the 2018 Twentieth International Middle East Power Systems Conference (MEPCON), Cairo, Egypt, 18–20 December 2018; pp. 948–955. [CrossRef]
20. Liu, Z.; Su, C.; Høidalen, H.K.; Chen, Z. A Multiagent System-Based Protection and Control Scheme for Distribution System with Distributed-Generation Integration. *IEEE Trans. Power Deliv.* **2017**, *32*, 536–545. [CrossRef]
21. Sampaio, F.C.; Leao, R.P.; Sampaio, R.F.; Melo, L.S.; Barroso, G.C. A multi-agent-based integrated self-healing and adaptive protection system for power distribution systems with distributed generation. *Electr. Power Syst. Res.* **2020**, *188*, 106525. [CrossRef]
22. Shirazi, E.; Jadid, S. A multiagent design for self-healing in electric power distribution systems. *Electr. Power Syst. Res.* **2019**, *171*, 230–239. [CrossRef]
23. Uzair, M.; Li, L.; Zhu, J.G.; Eskandari, M. A protection scheme for AC microgrids based on multi-agent system combined with machine learning. In Proceedings of the 29th Australasian Universities Power Engineering Conference (AUPEC), Nadi, Fiji, 26–29 November 2019.
24. Hojjaty, M.; Fani, B.; Sadeghkhani, I. Intelligent Protection Coordination Restoration Strategy for Active Distribution Networks. *IET Renew. Power Gener.* **2022**, *16*, 397–413. [CrossRef]
25. HOMER®Pro User Manual. Available online: www.homerenergy.com (accessed on 20 July 2023).
26. Hatata, A.Y.; Osman, G.; AlAdl, M.M. Design and Analysis of Wind Turbine/PV/Fuel Cell Hybrid Power System Using HOMER and Clonal Selection Algorithm. In Proceedings of the 2015 Seventeenth International Middle East Power Systems Conference (MEPCON), Mansoura, Egypt, 15–17 December 2015.
27. NASA. Surface Meteorology and Solar Energy. Available online: https://eosweb.larc.nasa.gov/sse/ (accessed on 20 July 2023).
28. Siemens. Gamesa Renewable Energy. Available online: https://www.siemensgamesa.com/en-int/products-and-services (accessed on 20 July 2023).
29. Lu, Z.; Lu, C.; Feng, T.; Zhao, H. Carbon dioxide capture and storage planning considering emission trading system for a generation corporation under the emission reduction policy in China. *IET Gener. Transm. Distrib.* **2015**, *9*, 43–52. [CrossRef]
30. Elsadd, M.A.; Yousef, W.; Abdelaziz, A.Y. New adaptive coordination approach between generator-transformer unit overall differential protection and generator capability curves. *Int. J. Electr. Power Energy Syst.* **2020**, *118*, 105788. [CrossRef]